UNIVERSIDAD DE INVESTIGACIÓN DE TECNOLOGÍA EXPERIMENTAL YACHAY

Escuela de Ciencias Químicas e Ingeniería

TÍTULO: Study of Electron Transport in DNA Model

Trabajo de integración curricular presentado como requisito para la obtención del título de Química

Autor:

Cardenas Gamboa Jorge Ivan

Tutor:

Ph.D. Solmar Alexandra Varela

Co-Tutor:

Ph.D. José Garcia

Urcuquí, February 2020

Urcuquí, 9 de abril de 2020

SECRETARÍA GENERAL
(Vicerrectorado Académico/Cancillería)
ESCUELA DE CIENCIAS QUÍMICAS E INGENIERÍA
CARRERA DE QUÍMICA
ACTA CONSOLIDADA DE FINALIZACIÓN DE ESTUDIOS No. UITEY-CHE-2020-00018-AC

En la ciudad de San Miguel de Urcuquí, Provincia de Imbabura, a los 9 días del mes de abril de 2020, se emite la presente acta consolidada de finalización de estudios, conforme lo establecido en el artículo 101 del Reglamento de Régimen Académico aprobado por el Consejo de Educación Superior (CES), mediante resolución RPC-SO-08-No.111-2019, de 27 de febrero de 2019.

DATOS DE IDENTIFICACIÓN DEL ESTUDIANTE

Documento de Identificación	Apellidos y Nombres	Carrera
0503738304	CARDENAS GAMBOA, JORGE IVAN	QUÍMICA

SUFICIENCIA DE LA LENGUA EXTRANJERA

Conforme lo establecido en el artículo 31 del Reglamento de Régimen Académico aprobado por el Consejo de Educación Superior (CES), mediante resolución RPC-SE-13-No.051-2013, de 22 de marzo de 2017: (…) las IES garantizarán el nivel de suficiencia del idioma para cumplir con el requisito de graduación de las carreras de nivel técnico superior, tecnológico superior y sus equivalentes; y, tercer nivel, de grado, deberán organizar u homologar las asignaturas correspondientes desde el inicio de la carrera. La suficiencia de la lengua extranjera deberá ser evaluada antes de que el estudiante se matricule en el último periodo académico ordinario de la respectiva carrera; tal prueba será habilitante para la continuación de sus estudios, sin perjuicio de que este requisito pueda ser cumplido con anterioridad. (…) En las carreras de tercer nivel, de grado, se entenderá por suficiencia en el manejo de una lengua extranjera al menos el nivel correspondiente a B2 del Marco Común Europeo de referencia para las Lenguas. (…)

Calificación	Nivel Alcanzado	Fecha Examen	Fecha Ingreso
101	C1	15/05/2019	03/06/2019

Mgs. MONTAÑO ORMAZA, DENNYS EDUARDO
Director del Departamento de Inglés

Firmado electrónicamente por:
DENNYS EDUARDO MONTANO ORMAZA

PRÁCTICAS PRE-PROFESIONALES O PASANTÍAS

Conforme lo establecido en los artículos 82, 89, 94 del Reglamento de Régimen Académico aprobado por el Consejo de Educación Superior (CES), mediante resolución RPC-SE-13-No.051-2013, de 22 de marzo de 2017.

Vinculación

Empresa	Nombre Proyecto	Horas	Fecha Inicio	Fecha Fin
UNIDAD EDUCATIVA VICTOR MANUEL GUZMAN	INSPIRATHON	160	06/03/2019	08/06/2019
	Total Horas Cumplidas:	**160**		

Prácticas

Empresa	Horas	Fecha Inicio	Fecha Fin
UNIVERSIDAD DE INVESTIGACIÓN DE TECNOLOGÍA EXPERIMENTAL YACHAY	240	01/10/2018	31/12/2018
UNIVERSIDAD DE INVESTIGACIÓN DE TECNOLOGÍA EXPERIMENTAL YACHAY	252	01/05/2018	31/07/2018
Total Horas Cumplidas:	**492**		

Firmado electrónicamente por:
BYRON VINICIO

Dr. MAZA ROJAS, BYRON VINICIO, Ph.D.
Coordinador de Servicios Escolares

REGISTRO DE CALIFICACIONES

Conforme lo establecido en el artículo 24 del Reglamento de Titulación de Grado de la Universidad de Investigación de Tecnología Experimental Yachay, en el que establece: La calificación final de grado del estudiante se obtendrá calculando de la siguiente manera: 1. El 70% corresponderá al promedio ponderado de calificaciones obtenidas por el estudiante a lo largo de toda su carrera y que se calculará en relación con el número de horas totales asignadas a cada asignatura en la correspondiente malla curricular distribuido así: a) El 20% para las asignaturas del "Tronco Común"; y, b) El 50% para las asignaturas propias de cada Carrera incluyendo los itinerarios. 2. El 30% restante corresponderá a la calificación de la defensa del trabajo de titulación o del examen teórico – práctico.

Fecha de Inicio: 20/04/2015 **Fecha de Finalización:** 09/04/2020

	Promedio	Horas	Créditos	Porcentaje	Calificación
Tronco Común	7,7			20 %	1,5
Carrera	8,6	8264	211	50 %	4,3
Defensa	10			30 %	3
			Calificación Final de Grado:	100 %	8,8

Firmado digitalmente por EDISON GUILLERMO CASANOVA YANDUN
Fecha: 2020.07.10 14:35:27 -05'00'

Mgs. CASANOVA YANDUN, EDISON GUILLERMO
Director de Registros Académicos

TITULACIÓN

Una vez se ha verificado el cumplimiento de los requisitos establecidos en el artículo 31 del Reglamento de Titulación de Grado de la Universidad de Investigación de Tecnología Experimental Yachay, aprobado mediante Resolución No.RCG-SE-10 No.036-2018 de 28 de septiembre de 2018, se confiere el título de **QUÍMICO/A**, a el(la) señor(ita) **CARDENAS GAMBOA, JORGE IVAN**.

Desde la fecha de suscripción de la presenta acta, conforme lo establecido en el artículo 101 del Reglamento de Régimen Académico aprobado por el Consejo de Educación Superior (CES), mediante resolución RPC-SO-08-No.111-2019, de 27 de febrero de 2019; la Universidad de Investigación de Tecnología Experimental Yachay, tiene un plazo de cuarenta y cinco (45) días para registrar el título en el Sistema Nacional de Información de la Educación Superior (SNIESE), previa entrega al graduado.

Para constancia de lo actuado, firman el Secretario General, el Decano de la Escuela y el/la Estudiante.

GRACIELA MARISA SALUM
Firmado digitalmente por GRACIELA MARISA SALUM
Fecha: 2020.07.11 12:27:35 -05'00'

Dra. SALUM, GRACIELA MARISA, Ph.D.
Secretaria General

CERTIFICACIÓN ELECTRÓNICA BANCO CENTRAL DEL ECUADOR
Firmado Digitalmente por: HORTENSIA MARIA RODRIGUEZ CABRERA
Hora oficial Ecuador: 10/07/2020 11:01

Dra. RODRIGUEZ CABRERA, HORTENSIA MARIA, Ph.D.
Decano

CARDENAS GAMBOA, JORGE IVAN
Estudiante

AUTORÍA

Yo, **JORGE IVAN CARDENAS GAMBOA**, con cédula de identidad 0503738304, declaro que las ideas, juicios, valoraciones, interpretaciones, consultas bibliográficas, definiciones y conceptualizaciones expuestas en el presente trabajo; así cómo, los procedimientos y herramientas utilizadas en la investigación, son de absoluta responsabilidad de el/la autora (a) del trabajo de integración curricular. Así mismo, me acojo a los reglamentos internos de la Universidad de Investigación de Tecnología Experimental Yachay.

Urcuquí, Juliodel 2020.

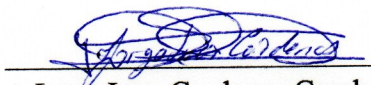

Jorge Ivan Cardenas Gamboa
CI: 0503738304

AUTORIZACIÓN DE PUBLICACIÓN

Yo, **JORGE IVAN CARDENAS GAMBOA,** con cédula de identidad 0503738304, cedo a la Universidad de Tecnología Experimental Yachay, los derechos de publicación de la presente obra, sin que deba haber un reconocimiento económico por este concepto. Declaro además que el texto del presente trabajo de titulación no podrá ser cedido a ninguna empresa editorial para su publicación u otros fines, sin contar previamente con la autorización escrita de la Universidad.

Asimismo, autorizo a la Universidad que realice la digitalización y publicación de este trabajo de integración curricular en el repositorio virtual, de conformidad a lo dispuesto en el Art. 144 de la Ley Orgánica de Educación Superior

Urcuquí, Julio del 2020.

Jorge Ivan Cardenas Gamboa
CI: 0503738304

Dedicatoria

Este trabajo de investigación quisiera dedicarlo a mis padres, Alba e Ivan y a mis hermanos Christian y Muriel. Todos ustedes son mi inspiración para seguir adelante y cada triunfo en mi vida es gracias a ustedes. Desde lo más profundo de mi corazón , los amo mucho, gracias por confiar en mi y apoyarme cada día en mis sueños y aspiraciones. Este solo es el comienzo de grandes cosas.

Jorge Ivan Cardenas Gamboa.

Agradedicimientos

Quisiera empezar agradiciendo a la Universidad de Investigación de Tecnologia Experimental Yachay Tech, mi alma máter quien forma jóvenes científicos motivados a cambiar la realidad social a través de la ciencia. Ser parte de una generación de científicos Ecuatorianos que van a cambiar el mundo es algo que jamás pensé podía ser parte y me siento muy orgulloso de serlo. Y de igual manera, un agradicimiento a la facultad de Ciencias Químicas e Ingeniería la cual me abrió las puertas a una enseñanza de calidad, con profesores de excelencia quienes me han motivado y guiado a seguir una carrera en ciencias, siempre llevaré en el corazón todo lo aprendido durante estos años.

A mi tutora, Solmar Varela. Gracias por recibirme como su estudiante, por mantenerme motivado y creer en mi. Usted ha sido una amiga, profesora y un ejemplo a seguir, lo cual me llevaré siempre como referencia en mi futra carrera científica. Gracias por darme la oportunidad de realizar este trabajo de investigación junto a usted.

A mi co-tutor, José García. Gracias por toda la paciencia durante este trabajo, desde la distancia usted ha sido un maravilloso profesor que siempre ha estado para solventar todas mis dudas y guiarme a culminar este trabajo.

Gracias a el profesor Manuel Caetano por abrirme las puertas al asombroso mundo de la Química Cuántica, mis primeros pasos en esta rama de la ciencia que estoy seguro que será mi futuro profesional como científico.

A Thibault Terencio y Floralba López, quienes han dedicado mucho tiempo y paciencia para guiarme en el camino correcto, especialmente a la profesora Floralba López por darme la oportunidad de realizar mis pasantías en Francia, la cual fue la mejor experiencia/reto que he tenido para aprender durante la universidad.

A todos mis amigos quienes me han apoyado en todo este camino durante la Universidad. Gracias por ser parte de mi vida "Casa 26". Un gracias muy especial a Jonathan

Barberan quien es y será un gran amigo en mi vida, quién constantemente me motiva a seguir mis sueños. Además quisiera agradecer a Jocelyne Estrella, nunca olvidaré todas las noches escuchando Silvio Rodriguez y estudiando, aprendimos mucho juntos y espero seguir apoyandote durante todo el transcurso que nos sigue como profesionales. A mi familia y a todo aquel que cree en mí y apoya este sueño que estoy construyendo junto a ustedes.

Gracias, muchas gracias a todos.

Jorge Ivan Cardenas Gamboa.

Abstract

In this work, we use the Landauer-Buttiker formula as implemented in the package KWANT (Python library) for studying quantum transport in a DNA molecule based in an analytical tight-binding Hamiltonian recently developed. In our simulation, we used a Hamiltonian considering a kinetic term, a term for intrinsic Spin-Orbit (SO) interaction related to the atomic SO coupling, and a Rashba interaction due to the electric dipoles associated with hydrogen bonds between the bases of the double strand of DNA and we tested the effect of magnetic and no-magnetic leads in the spin-selectivity of the molecule. We obtained that in our model, the spin-orbit coupling associated with the molecule can not be enough to explain the spin selectivity, however, in a system with presence of ferromagnetic leads, enhance the spin selectivity when it is included, which could explain the selectivity observed in similar experiments

Keywords: DNA, Spin selectivity, Intrinsic spin-orbit, Rashba interaction, Tight-bindig model.

Resumen

En este trabajo, utilizamos la fórmula Landauer-Buttiker implementada en el paquete KWANT (biblioteca de Python) para estudiar el transporte cuántico en una molécula de ADN basada en un Hamiltoniano analítico de enlace fuerte recientemente desarrollado. En nuestra simulación, utilizamos un hamiltoniano considerando un término cinético, un término para la interacción intrínseca Spin-Orbit (SO) relacionada con el acoplamiento atómico de SO, y una interacción Rashba debido a los dipolos eléctricos asociados con enlaces de hidrógeno entre las bases del doble hebra de ADN y probamos el efecto de cables magnéticos y no magnéticos en la selectividad de giro de la molécula. Obtuvimos que en nuestro modelo, el acoplamiento espín-órbita asociado con la molécula no puede ser suficiente para explicar la selectividad del espín, sin embargo, en un sistema con presencia de cables ferromagnéticos, mejorar la selectividad del espín cuando se incluye, lo que podría explicar la selectividad observada en experimentos similares.

Palabras clave: ADN, Selectividad de spin, Interacciones spin-orbita , Interacciones Rashba, Modelo de enlace fuerte.

CONTENTS

Contents **vii**

Introduction **1**

0.1 General and specific objectives 8

1 Theoretical frame **9**

1.1 Quantum Transport 9

1.1.1 Drude's model 9

1.1.2 Electron conductivity and Ohm's law 11

1.1.3 Characteristic lengths 14

1.1.4 Buttiker-Landauer formalism 17

1.2 TIGHT BINDING 20

1.2.1 Tight binding approximation 21

1.3 KWANT software 23

1.4 Atomic interactions 25

1.4.1 Atomic Spin-Orbit interaction 25

1.4.2 Rashba effect 29

1.5 DNA MODEL 30

2 Results **34**

2.1 Linear chains 34

2.1.1 1D case 34

2.1.2 2D case 36

2.1.3 Regimen of Transport 38

2.2 3D DNA MODEL 39

2.2.1 No ferromagnetic leads, with and without SO interaction 42

2.2.2 Ferromagnetic leads, with and without SO interaction 45

Conclusions **48**

A APPENDIX **50**

A.1 Appendix 1 50

A.2 Appendix 2 53

A.3 Appendix 3 55

Bibliography **57**

INTRODUCTION

When we talk about technology, related to data processing, it is always related to the concept of transistors. Transistors are electronic devices that are capable of providing an arbitrary output to a given input. That is, transistors are responsible for translating human-generated outputs, such as sound, or to the electrical inputs that a computer needs to operate.[1].The first transistors were built by combining semiconductor materials to produce a nonlinear electrical response.From that moment, how to tune such a response for different purposes was the main subject of research since the 50s, and it remains to change and to innovate for different purposes until now.[2].

Transistors' technology has evolved through various phases, in rough correspondence with each decade after its invention. Through experiments seeking understanding and use of surface physics in germanium, John Bardeen, Walter Brattain, and William Shockley found the transistor effect and invented the point-contact transistor in 1947 [3]. These transistors consisted of a block of germanium, a semiconductor, with two very closely spaced gold contacts held against it by a spring. The surface layer of the germanium piece of the transistor had an excess of electrons, so when an electrical signal travels through the gold foil, it injected holes (points which lack electrons) creating a thin layer which had a scarcity of electrons or well known as transistor (Figure 0.1 a.). As a result of this

success the Nobel Prize committee joined the contributions, and awarded the contributors a single prize to the trio of scientist, Bardeen, Brattain, and Shockley pictured in Fig 0.1 b, opening the doors to a new era of the technology in which the use of transistors have been the key to more advanced technology.[2].

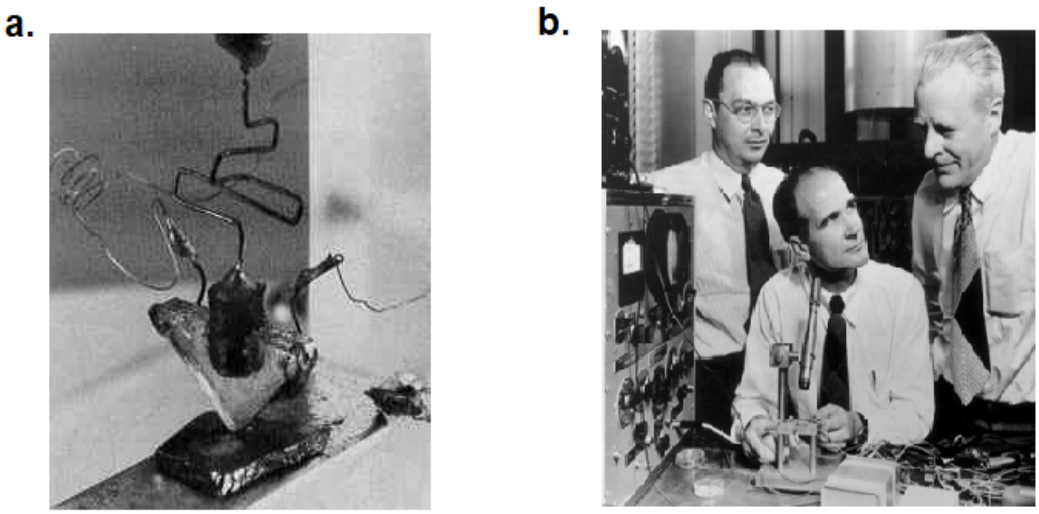

Figure 0.1: **a.** The small dark rectangle on the formed metal support at lower left center is polycrystalline germanium. The triangle impinging on it is an insulator with metal on near and far surfaces. **b.** Inventors of the transistor John Bardeen, William Shockley, and Walter Brattain (left to right) [3]

The first transistor, initially rustic and very primitive, has evolved over the years, the of use of sensors that respond to a stimulus can be applied in many areas of science and mainly being applied in technology. Sensitive, selective, miniaturized, light-weight, low-power biosensing systems should be capable of providing information to the user wherever and whenever it is needed. In a more visionary scenario, the more advanced transistors constructed at nanometric scale for their application in systems, would provide the correct information for specific cases, on which it is required [1]. To perform this kind of transistors the aim is to be able to elaborate transistors at nanometric scale, look for their application in technology, medicine, computers, and electronics.

An example of transistors developed nowadays is the Organic Field-Effect Transistors

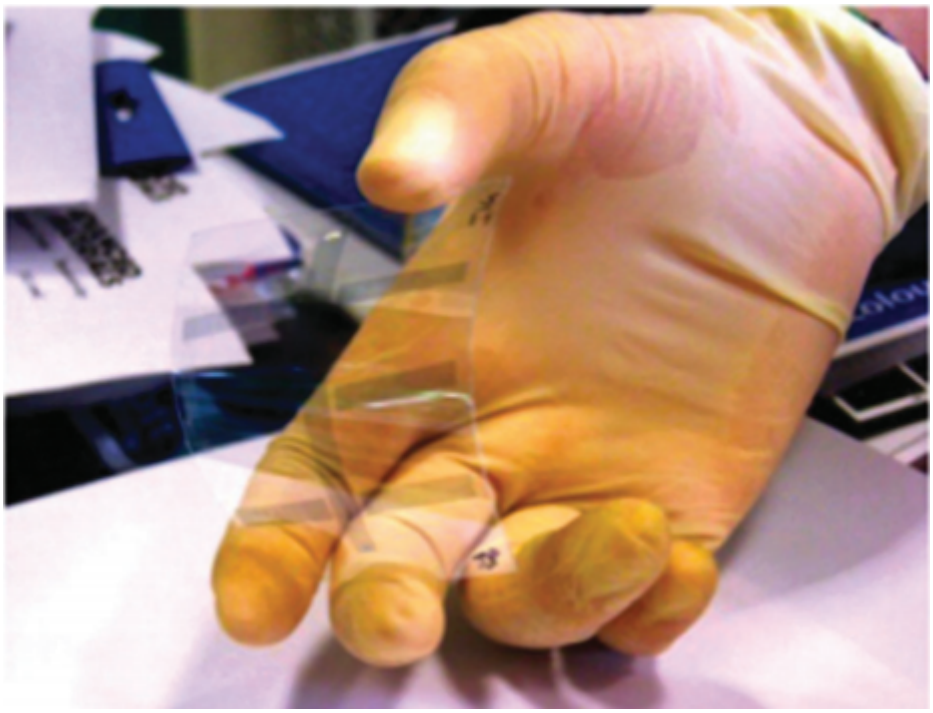

Figure 0.2: Picture of transparent and flexible OFETS. [4]

(OFET) sensors, highlighting the features that would make them ideal for POC (point of contact) applications. As the electrochemical OFET sensing configurations have an extensive range of sensors will be focus are on electrolyte and back-gated OFETs biosensors. In general OFET sensors use π-conjugated organic semiconductors as electronic materials and are endowed with biological recognition capabilities by proper functionalization or integration of bio-systems such as DNA strains, antibodies, enzymes and capturing proteins in general. The advantages of these OFET over other sensing technologies, such as electrochemical or optical-based ones, is the capability of delivering a response that is label-free using a simple electronic read-out set-up that can be easily miniaturized by also employing printed circuit technologies [1].

The revolutionary concept that is now turning into real prototypes, involves the construction of electronic and opto-electronic functional devices (light-emitting diodes, photovoltaic cells, OFETs) and circuits by printing features on plastic or paper substrates using dielectric, conducting, insulating and semiconducting inks. Plastic electronic systems are

produced at very low-cost using printing equipment instead of ultraclean high-tech fabrication facilities. The emerging field of organic electronics is therefore motivated by the possibility of mass-producing cheap and sustainable electronic devices and sensors. In Fig. 0.2 an example of inkjet printed, transparent OFETs on a flexible substrate, is featured [4].

One of the interesting properties of these devices, very useful at the application level, is their *ferromagnetism*, implying a strongly magnetic behavior, that is the strong attraction of a material to a permanent magnet. The origin of this strong magnetism is the presence of a spontaneous magnetization produced by a parallel alignment of spins. Also, there can be an anti-parallel alignment of unequal spins resulting in a spontaneous magnetization. Magnetic materials which are magnetized to some extent by a magnetic field. The use of the alignment of spin have been used in many materials due to that once known the magnetic orientation of a material many properties can be enhanced [5]. These materials have been used for many years, however chiral organic molecules are opening new doors as spin filters for applications in technology and computation [6].

Chiral are those that do not overlap onto their mirror image, such as the left hand and the right hand, are said to be [7]. Because many biomolecules are chiral and many biochemical reactions involve chiral molecules, much effort has been spent in the understanding of enantioselectivity in chemical transformations and in the study of the physical chemical properties of these structures [8]. Several experiments have demonstrated that the electron transmission yield through chiral molecules depends on the electron spin orientation. Groundbreaking experiments have shown strong spin selectivity (60% in some cases) in biological single molecules of DNA, photosystems, and bacteriorhodopsin, self-assembled monolayers of DNA and chiral oligopeptides [9]. One of the most important experimental results is the fact that spin selectivity is unequivocally linked to the chiral nature of the molecules, since the lack of it kills any spin activity in low atomic weight systems. This dependence of the selectivity with the chirality is known as Chiral-Induced Spin Selectivity effect, or CISS effect. [10, 11, 12, 13]

One of the first studies in spin selectivity are performed by Rikken and Raupauch, in which they report the first use of static magnetic field to bias a chemical process in favour of one of two mirror-images products (left or right handed eniantomer). Rikken and Raupach used magneto-chiral dichroism, associated to the production of one enantiomer in a photochemical reaction of the chiral Cr(III)tris-oxalato complex, which is unstable in solution and spontaneously dissociates and re-associates. At equilibrium the right and left handed enantiomers are at the same concentration. The dissociation of the chiral complex is accelerated by the absorption of light, such that in the presence of an unpolarized laser beam travelling parallel to a static magnetic field, a small excess of one enantiomer is produced and maintained and, on reversing the magnetic field direction, an equal concentration of the mirror-image enantiomer is obtained [8].

In more recent experiments, the CISS effect was experimentally studied in the tunnel effect energy regime by Zoutie Xie et al colaborators [14], through measurements of conductance of double-stranded DNA molecules. In that experiment, the DNA molecules

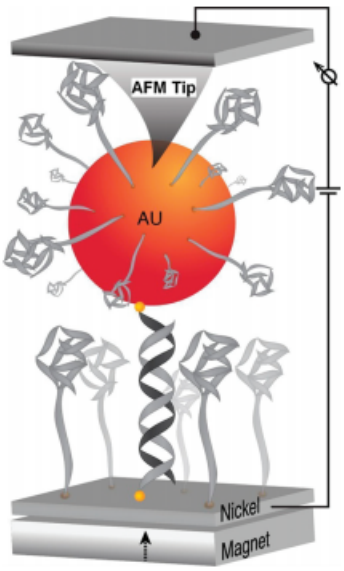

Figure 0.3: Experimental setup. A self-assembled monolayer of dsDNA on the gold nanoparticle is complementary to that SAM (self-assembled monolayer). The two strands hybridize to form a nanoparticle-dsDNA-nickel complex [14].

were deposited on a nickel substrate and attached at the other end to a gold nanoparticle, such that a gold nanoparticle-dsDNA-nickel complex type system was formed (see Figure 0.3). The dsDNA oligomers are bound on one end to the nickel surface (bottom electrode) while their outer ends are chemically bound to the gold nanoparticles (top electrode). Geometric constraints dictate that underneath each of the gold nanoparticles no more than two molecules can hybridize. A permanent magnet underneath the nickel substrate controlled the magnetism, and hence the spin alignment in the nickel. A conductive AFM was used to measure the current flowing between the nickel substrate through the DNA to the gold nanoparticles [14].

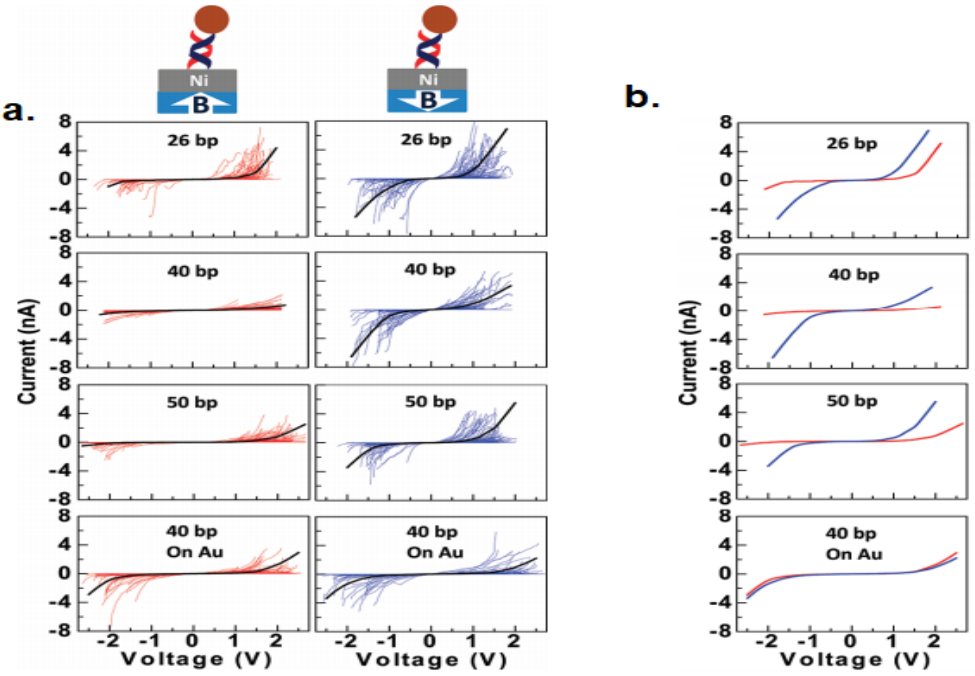

Figure 0.4: Current versus voltage curves obtained for the 50, 40 and 26 base pair (bp) long DNA oligomers absorbed on Ni. (a.) Current vs voltage for magnet pointing up and down (b.) The average current obtained for the three oligomers studied when the magnetic field is pointing up (red) or down (blue) [14]

The I-V curve measurement performed for different nickel magnetization are shown

in Figure 0.4. for these constructs formed by 26, 40 and 50 base-pairs (bp) long dsDNA, these magnet pointing up and down for each measurement as is observed in Figure 0.4 (part a.). The curves obtained are symmetrical, which means that regardless of the voltage applied, the spin is always antiparallel to the direction of movement of the electrons. This imply that while one spin is dominant in the transport when electrons are flowing away from the Ni, the opposite spin is dominant for the electrons flowing from the tip of the AFM toward the Ni. The symmetric structure also indicates that the magnetic field of the permanent magnet does not affect the current flow through the DNA in a significant way, but indeed affects only the spin alignment in the Ni substrate which is observed clearly in figure 0.4 (part b.), which shows the average values for conductance as a function of the applied voltage. Then, the dependence on the conductance of the molecule with the direction of the applied magnetic field and with the length of the molecule is obtained which is referred to a kind of spin filter in the DNA molecule.

In order to understand the experimental results obtained, many theoretical approaches have been developed taking spin-orbit and chirality of the molecule as main factors present in the structure. Solmar Varela et al Co-workers have developed a Tight-Binding (TB) model describing spin filtering and chiral spin transport through DNA model. The TB model incorporates both kinetic and intrinsic spin-orbit (ISO) contributions as well as Rashba-type interactions coupled to an external electric field along the axis of the double helix. The helical structure of the molecule renders the ISO first order in the interaction strength (in the meV range) as in carbon nanotubes[9].

As expected, depending on the complexity of the molecule, analytical calculation can become a difficult task. It is for this reason that the computational tool based on binding models is used as a complement to help describe this type of models and connect the theory with the experiments, which will allow in the future the application of these chiral molecules in technological development in which the use of inorganic materials is arriving to its limits. For this purpose, the use of KWANT (python library) focused on quantum transport is a computational tool that will allow us to study the mechanism of transport

in this molecule through TB models.

0.1 General and specific objectives

Taking into account the considerations mentioned above it is proposed as a general objective the **Study of the electron transport in a DNA model using KWANT to obtain conductance values in the molecule.** The specific objectives are:

1. Develop a simulation of DNA molecule using KWANT, a python library focused on conductance.
2. Analyze the results obtained with the program for our tight-binding model with the calculus proposed on 2016 by Solmar Volmar, Ph.D..
3. Demostrate the importance of computational tool in this kind of problems.

This thesis is organized into 2 chapters, conclusions, appendixes, and bibliography. In Chapter 1 is introduced important concepts to understand the conduction of electron in materials, from the beginning to the formalism used in KWANT. Then is described the different interactions that can be present in the system and finally the DNA model used to perform the simulation developed in this work. In Chapter 2 is shown some examples and an easy introduction to KWANT using the simple tight-binding model in 1D and 2D for visualize the resulting conductance and band structure, for explaining each one with the other. Furthermore, we present results obtained with the DNA model using the spin-orbit interactions and ferromagnetic lead, and by this way, explaining the conductance, the band structure and the spin-selectivity present in the molecule. In appendix section A are shown some codes used for the cases studied in Chapter 2. For the A.1 is shown the codes used for a linear chain, in A.2 is shown the code used for a 2D system and finally in A.3 is shown some parameters used for the development of the DNA model explained in 2.2. Finally, thesis work is concluded pointing out the most important results that we find using KWANT and closed with the Bibliography.

CHAPTER 1

THEORETICAL FRAME

1.1 Quantum Transport

1.1.1 Drude's model

Even in ancient times it was understood that certain substances (now known as metals) were somehow different from other materials in the world. The defining characteristic of a metal is that it conducts electricity. At some level the reason for this conduction boils down to the fact that electrons are mobile in these materials.

J.J. Thomson's 1896 discovery of the electron ("corpuscles of charge" that could be pulled out of metal) raised the question of how these charge carriers might move within the metal. In 1900 Paul Drude realized that he could apply Boltzmann's kinetic theory of gases to understanding electron motion within metals. This theory was remarkably successful, providing a first understanding of metallic conduction. Furthermore, three main assumptions were made:

1. Electrons have scattering time τ. The probability of scattering within a time interval dt is dt/τ

2. One a scattering event occurs, it is assumed that the electron returns to zero-momentum $p = 0$. This is true on average but not for every particle, so this is a defect of the model.

3. In between scattering events, the electrons, which are charge $-e$ particles, respond to the externally applied electric field $\mathbf{E}$ and magnetic field $\mathbf{B}$. [15]

The first two assumptions are exactly those made in the kinetic theory of gases. while the third assumption is just a logical generalization to account for the fact that, unlike gas molecules, electrons are charged and therefore they must respond to electromagnetic fields [15].

Considering an electron with momentum p at time t and ask what momentum it will have at time $t+dt$. There are two terms in the answer. There is a probability dt/τ that it will scatter to momentum zero. If it does not scatter to momentum zero (with probability $1 - dt/\tau$) it simply accelerates as dictated by its usual equation of motions $dp/dt = \mathbf{F}$. Putting the two terms together we have:

$$\langle p\,(t + dt)\rangle = (1 - \frac{dt}{\tau})(p(t) + F dt), \tag{1.1}$$

or keeping terms only to linear order in dt, and then rearranging it is obtained:

$$\frac{dp}{dt} = F - \frac{p}{\tau}, \tag{1.2}$$

where the force $\mathbf{F}$ on the electron is given by the Lorentz force:

$$\mathbf{F} = -\mathbf{e}(\mathbf{E} + \mathbf{v} \times \mathbf{B}).$$

In this last equation $\mathbf{E}$ and $\mathbf{B}$ have the same meaning given before, and v is the velocity and e is the charge electron.

The scattering term $-p/\tau$ ca be associated with a drag force on the electron. Notice that in the absence of any externally applied field the solution to the differential equation

is just an exponentially decaying momentum

$$p(t) = p_{inital} e^{-t/\tau},$$

which is expected for particles that lose momentum by scattering [16].

1.1.2 Electron conductivity and Ohm's law

Electrical conduction is a process by which an electron travels a certain distance experiencing a series of scattering events. Recent advances in technology have made it possible to fabricate structures whose dimensions are much smaller obtaining a better conduction, applicability and use in different devices [17]. Quantum Mechanics Principles provide the tools which describe how this process is happening opening the doors to the new era of nanodevices. The phenomena of conduction that present solid structures can be of many kinds, from quantum characteristic to structural description. However in this case we are going to be focused on quantum transport of electrons and its spin polarization.

Conductance is defined as electric current passing through a solid system. The conductance (G) of a rectangular two-dimensional conductor is directly proportional to its width (W) and inversely proportional to its length (L) (Figure 1.1) [18]:

$$G = \frac{\sigma * W}{L}, \tag{1.3}$$

where, σ is the conductivity measured in ($\frac{S}{cm^2}$). As shown in the equation (1.3), the conductance is directly proportional to sigma "σ" which is called *conductivity* and refers to an intrinsic value for each material, which shows the measure of electrical charge or heat can pass through a material, then at a higher value of "σ" the conductivity and the conductance would be higher.

The momentum of a free electron is related to the wave vector by $mv = \hbar k$, where m and v are the electron mass and velocity, respectively. In an electric field $\mathbf{E}$ and magnetic

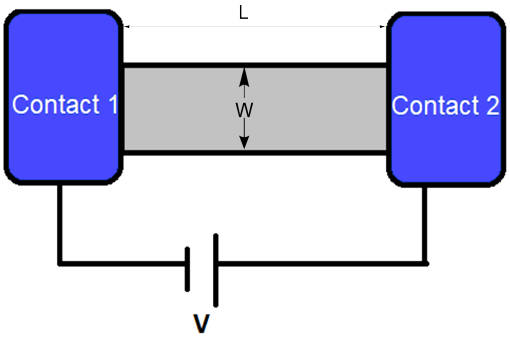

Figure 1.1: A conductor is switched between two contacts across which an external field bias is applied.

field $\mathbf{B}$, the force $\mathbf{F}$ on an electron of charge $-e$ is $-e[\mathbf{E}+\mathbf{v}\times\mathbf{B}]$, such that the Newton's second law of motion becomes:

$$F = m\frac{dv}{dt} = \hbar\frac{dk}{dt} = -e(\mathbf{E}+\mathbf{v}\times\mathbf{B}). \tag{1.4}$$

As shown in Figure 1.2, the Fermi sphere which represents the available states in the system, moves in $\mathbf{k}$ space at a uniform rate by a constant applied electric field. By integration of 1.4 with $\mathbf{B}=\mathbf{0}$ it is obtained:

$$k(t) - k(0) = -eEt/\hbar. \tag{1.5}$$

If the force $\mathbf{F}=-\mathbf{eE}$ is applied at time $t=0$ to an electron gas that fills the Fermi sphere centered at the origin of $\mathbf{k}$ space, then at a latter time t the center of the sphere will be displaced to :

$$\delta k = -eEt/\hbar. \tag{1.6}$$

Notice that the Fermi sphere is displaced as a whole because every electron is displaced by the same $\delta\mathbf{k}$.

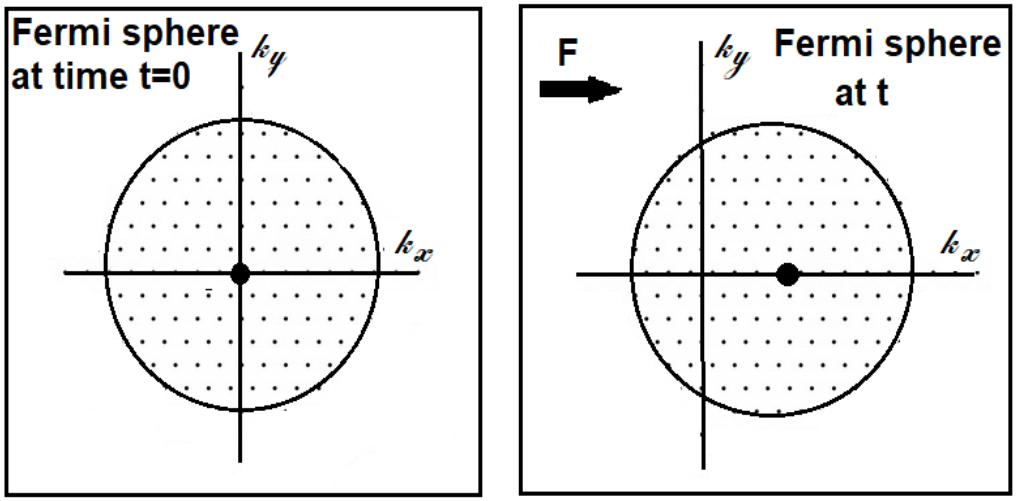

Figure 1.2: **(a.)** The Fermi sphere encloses the occupied electrons orbitals in **k** space in the ground state of the electron gas. The net momentum is zero, because for every orbital **k** there is an unoccupied orbital at **-k**. **(b.)** Under the influence of a constant force **F** acting for a time interval t every orbital has its **k** vector increased by $\delta\mathbf{k}$, this is equivalent to a displacement of the whole Fermi sphere by $\delta\mathbf{k}$ [15].

Because of collision of electrons with impurities, lattice imperfections, and phonons, the displacement of the sphere may be maintained in a steady state of the electric field. If the collisions time is τ, the incremental velocity is $\mathbf{v}\delta\mathbf{k}/m = -\mathbf{e}\mathbf{E}\tau/m$. If in a constant electric field **E** there are n electrons with charge $q = -e$ per unit of volume, the electric current density is:

$$j = nqv = \frac{ne^2\tau E}{m}. \tag{1.7}$$

The equation (1.7) is known as **Ohm's law**. The electrical conductivity σ can be written in term of $j = \sigma E$, such that (1.7):

$$\sigma = \frac{ne^2\tau}{m}, \tag{1.8}$$

and at the same way, the electrical resistivity ρ is defined as the reciprocal of the conductivity:

$$\rho = \frac{m}{ne^2\tau}. \tag{1.9}$$

The time τ describes the free time during which the field acts on the carrier. Closely the same result for the electrical conductivity is obtained for a classical (Maxwellian) gas of electrons, as realized at low carrier concentration in many semiconductors problems [15].

Therefore, conductance is defined as the measurement of electrons passing through a system. This conductance is related to the geometry of the system that is being applied for its dimensions either by its length or width and the most important by the nature of the material itself.

1.1.3 Characteristic lengths

A conductor usually shows ohmic behavior if its dimensions are much larger than certain characteristics lengths: the de Broglie wavelength, the mean free and the phase-relaxation length.

1.1.3.1 Wavelength (λ)

The relation between the Fermi wavenumber (k_f) and the density of states (n_s) is given by:

$$k_f = \sqrt{2\pi n_s}. \tag{1.10}$$

Then, the Fermi wavenumber (λ_f) goes up as the square root of the electron density. The corresponding wavelength goes down as the square root of the electron density down as the square root of the electron density:

$$\lambda_f = 2\pi/k_f = \sqrt{2\pi/n_s}. \tag{1.11}$$

As an example, for an electron density of $5 \times 10^{11}/cm^2$, the Fermi wavelength is about 35 nm. At low temperatures the current density is carried mainly by electrons having an energy close to the Fermi energy, so that the Fermi wavelength is the relevant length. Other electrons with less kinetic energy have longer wavelengths but they do not contribute to the conductance wavelengths [18].

1.1.3.2 Mean free Path (L_m)

An electron in a perfect crystal moves as if it were in vacuum but with a different mass. Any deviation from perfect crystallinity, such as presence of impurities, lattice vibrations (phonons) or other electrons lead to 'collisions' that scatter the electron from one state to another thereby changing its momentum. The momentum relaxation time τ_m is related to the collision time τ_c by a relation of the form:

$$\frac{1}{\tau_m} \Rightarrow \frac{1}{\tau_c}\alpha_m,$$

where the factor α_m (lying between 0 and 1) denotes the 'effectiveness' of an individual collision in destroying momentum.

The mean free path L_m, is the distance that an electron travels before its initial momentum is destroyed, it is defined by:

$$L_m = v_f \tau_m, \tag{1.12}$$

where τ_m is the momentum relaxation time, and v_f is the Fermi velocity given by:

$$v_f = \frac{\hbar k_f}{m}, \tag{1.13}$$

which, using 1.11 can be written as:

$$v_f = \frac{\hbar}{m}\sqrt{2\pi n_s}. \tag{1.14}$$

1.1.3.3 Phase-relaxation length (L_φ)

Another characteristic length that should be considered is the phase-relaxation length. An equation (or definition) for phase relaxation time (τ_φ) can be written as:

$$\frac{1}{\tau_\varphi} \Rightarrow \frac{1}{\tau_c}\alpha_\varphi,$$

where the factor α_φ denotes the effectiveness of an individual collision in the destroying phase. One way to visualize the destruction of phases in terms of a thought experiment involving interference is for example supposed the case of a splitting a beam of electrons into two paths and then recombine them as shown in Fig 1.3.

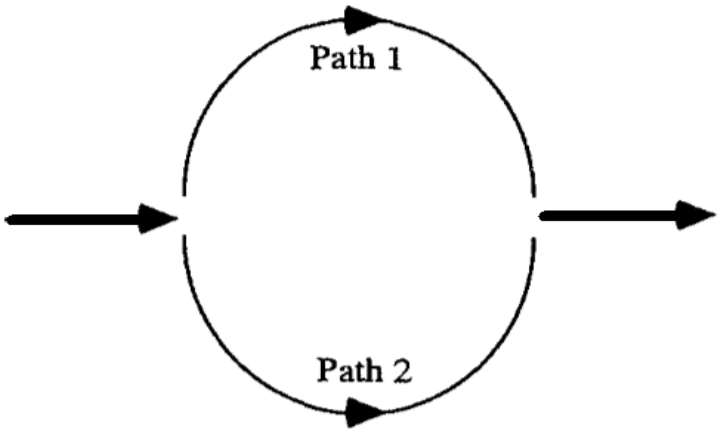

Figure 1.3: A conceptual interference experiment involving the splitting of a beam of electrons and later recombining them. [18]

In a perfect crystal the two paths would be identical resulting in constructive interference. By applying a magnetic field perpendicular to the plane containing the paths, one can change their relative phase alternately from constructive to destructive. Now suppose we are not in a perfect crystal but in a real one with collisions due to impurities, phonons etc. It would expect the interference amplitude to be reduced by a factor $exp[-\tau_t/\tau_\varphi]$, where τ_t is the transit time that the electron spends in each arm of the interferometer.

1.1.4 Buttiker-Landauer formalism

Landauer formula describes a ballistic or quasi-ballistic conduction through a simple two-dimensional configuration [17]. Let us consider a piece of a conductor stretched between two large contact pads as is shown in Figure 1.1. To determine the conductance of this semiconductor, taking as supposition that it presents impurities, Landauer allows to determine the conductance by the following equation:

$$G = \left(\frac{2e^2}{h}\right) MT \tag{1.15}$$

where e, h, and M are the electron charge, the Planck's constant and the number of modes, respectively. The factor T represents the average of probability that an electron injected at the end of the conductor will transmit to the other end . If the transmission probability is the unit, we recover the correct expression for the resistance of a ballistic conductor in which it is not present any scattering[18]. Now, considering a even more complicated system like Figure 1.4, representig to a conductor connected to two large contacts by two leads.

The leads are described as ballistics, a behavior as a metallic material (no scattering) is assumed, and each one of them have M modes. As in the previous example, T is the average probability of inject an electron inside the channel. As is supposed each electron pass through the channel without reflection, they are called 'reflectionless'. Then, states in the lead 1 are electrons coming from the left contact correspond to $+k_x$, and hence these states must have an electrochemical potential μ_1, indicated in the Figure 1.4, similarly, it is argued the same for the state $-k_x$ assuming a electrochemical potential μ_2. Assuming the ideal case (zero temperature), the current flow I_1^+ and I_2^+ will be proportional to the voltage μ_1 and μ_2.

Then the influx of the electrons in the lead 1 is given by:

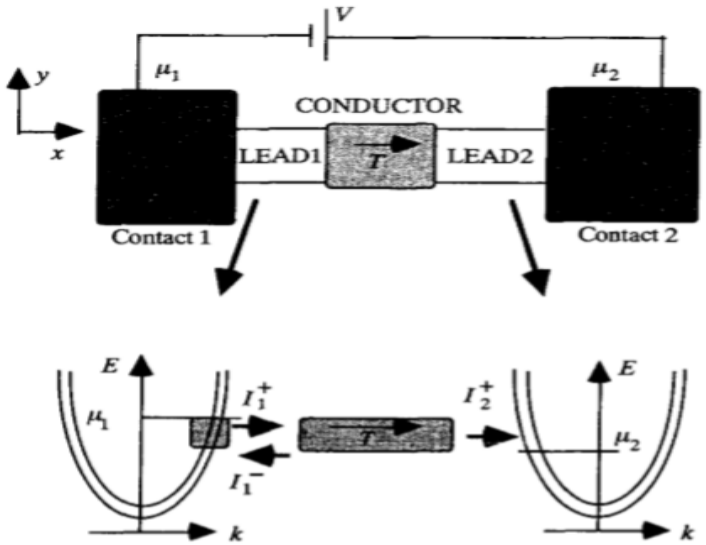

Figure 1.4: A conductor having a transmission probability of T is connected to two large contacts through two leads. [18]

$$I_1^+ = (2e/h)M[\mu_1 - \mu_2]. \tag{1.16}$$

The outflux from lead 2 is simply the influx at lead 1 times the transmission probability T:

$$I_2^+ = (2e/h)MT[\mu_1 - \mu_2]. \tag{1.17}$$

The rest of the flux is reflected back to contact 1:

$$I_1^- = (2e/h)M(1-T)[\mu_1 - \mu_2] \tag{1.18}$$

Then, the net I current passing from one lead to another at any point of the device is given by:

$$I = I_1^+ - I_1^- \approx I_2^+ = (2e/h)MT[\mu_1 - \mu_2]. \tag{1.19}$$

Hence, from Landauer formalism that the conductance can be assumed as:

$$G = \frac{I}{(\mu_1 - \mu_2)|e|} = \frac{2e^2}{h} MT. \tag{1.20}$$

The electron dynamics of a bulk material composed of large ensembles of particles can be calculated by averaging over many microscopic configurations. Although the quantum behavior of individual constituents of a macroscopic object are important over some lengths scale, typically a few lattice spacing, they are usually not correlated across the whole object [19]. As can be expected, in a system with no defects the conduction of electrons cross the channel without any problem through it, however, in disordered systems the electrons will be scattered by many factors, such as presence of impurities, loosing some electrons which are traveling through channel. Then, if this disorder is high enough, it will lead to interferences of the electronic wave function $\psi(x)$ with itself, such that it is no longer extended over the whole solid but is instead confined to a small part of the solid [20]. This phenomenon is known as *Anderson localization*. Depending on the type of system studied , three different quantum regimes can exist:

1. Ballistic: the canonical example is the point contact; impurity scattering can be neglected, and electron scattering occurs only at boundaries.

2. Diffusive: conducting samples contain a significant amount of impurity atoms or structural disorder. The strength and concentration of impurities leads to $l \sim 100$ Å, which is the elastic scattering length, independent of temperature.

3. Localized: when the disorder is strong enough, a phenomena known as Anderson localization take place.

To understand these regimes, in 1972 were proposed a highly successful theoretical approach to this disorder-induced made by Abrahams[20]. The starting point for his approach is the realization that there exists a sample-size (L^d) dependence of the conductance is given by:

$$G = \sigma L^{d-2} = g\frac{e^2}{\hbar}. \tag{1.21}$$

On the other hand, for strong disorder, the wave functions will be exponentially localized with localization length λ and thus the conductance in a finite system will be:

$$g \sim exp(\frac{-L}{\lambda}). \tag{1.22}$$

As is expected as numerical as in theory the relationship between the conductance and the length is a exponential decay.

1.2 TIGHT BINDING

The tight binding or linear combination of atomic orbitals (LCAO) method is a semi-empirical method that is primarily used to calculate the band structure and single-particle Bloch states of a material. The semi-empirical tight binding method is simple and computationally very fast. It therefore tends to be used in calculations of very large systems, with more than around a few thousand atoms in the unit cell [21].

To understand how this method works, lets start with neutral separated atoms and watch the changes in the atomic levels as the charge distribution of adjacent atoms overlap when the atoms are brought together to form a crystal. Consider two hydrogen atoms, each with an electron in the ground state. The wavefunctions ψ_A , ψ_B on the separated atoms are shown in Figure 1.5, A). As the two atoms are brought together, their wavefunctions overlap (see Figure 1.5, B). Considering the combination of both $\psi_A \pm \psi_B$, then each combination share an electron with two protons, but an electron in the state $\psi_A + \psi_B$ will have a somewhat lower energy than in the state $\psi_A - \psi_B$. In $\psi_A + \psi_B$ the electron spend part of the time in the region midway between the two protons, and in this region it is in the attractive potential of both protons at once, thereby increasing the binding energy . In $\psi_A - \psi_B$ the probability density vanishes midway between the nuclei, an extra binding does not appear.

As two atoms are brought together, two separated energy levels are formed for each level of the isolated atom. For N atoms, N orbitals are formed for each orbital of the

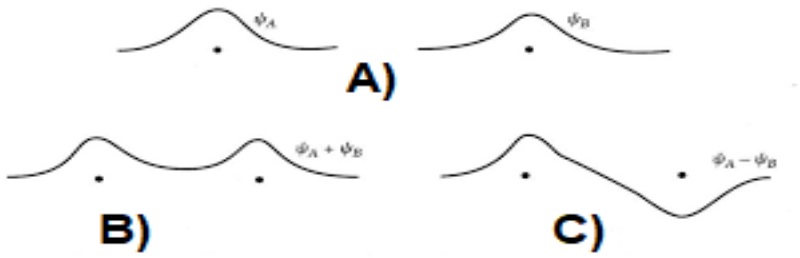

Figure 1.5: **A.** Schematic drawing of wavefunctions on two hydrogen atoms at large separation. **B.** Ground state wavefunctions at closer separation. **C.** Excited wavefunctions. [15]

isolated atom, as is observed in Figure 1.6. As free electrons are brought together, the Coulomb interaction between the atom cores and the electron splits the energy levels, spreading them into bands. Each state of given quantum number of the free atom is spread in the crystal into a band of energies. The width of the band is proportional to the strength of the overlap interaction between neighboring atoms [15].

1.2.1 Tight binding approximation

Suppose that the ground state of an electron moving in the potential $\mathbf{U}(\mathbf{r})$ of an isolated atom is $\varphi(r)$, an **s** state. If the influence of one atom on another is small, we obtain an approximate wavefunction for one electron in a whole crystal by taking

$$\psi_k(r) = \sum_j C_{kj}\varphi(r - r_j), \tag{1.23}$$

where k is the wave vector of the electron and the sum is over all lattice points. The assumptions made is that primitive basis contains one atom. This function has a Bloch form, if $C_{kj} = N^{-1/2}e^{i\mathbf{k}\cdot\mathbf{r}}$, which gives, for a crystal of N atoms, the following equation:

$$\psi_k(r) = N^{-1/2}\sum_j exp(i\mathbf{k}\cdot\mathbf{r}_j)\varphi(r - r_j) \tag{1.24}$$

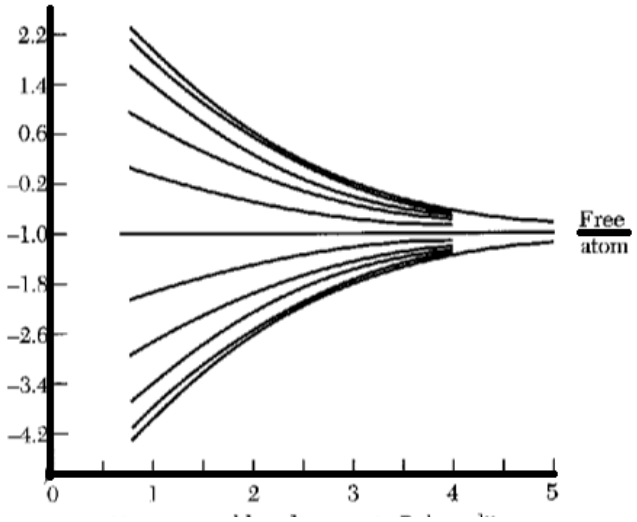

Figure 1.6: The 1s band of a ring of 20 hydrogen atoms. The one-electron energies are calculated in the tight-binding approximation. [15]

The first order-energy is calculated by getting the diagonal matrix elements of the hamiltonian of the crystal, as the following:

$$\langle k \mid H \mid k\rangle = N^{-1}\sum_{j}\sum_{m} exp[i\mathbf{k}\cdot(\mathbf{r}_j - \mathbf{r_m})]\langle\varphi_m \mid H \mid \varphi_j\rangle, \tag{1.25}$$

where $\varphi_m \equiv \varphi(r - r_m)$. Writing $\rho_m = (r - r_j)$ we obtain:

$$\langle k \mid H \mid k\rangle = \sum_{m} exp(-ik\cdot\rho_m)\int dV\varphi^*(r-\rho_m)H\varphi(r). \tag{1.26}$$

Neglecting all the integrals in equation (1.26) except for those on the same atom and those between nearest neighbor connected by ρ, we write:

$$\int dV\varphi^*(r-\rho_m)H\varphi(r) = -\alpha; \int dV\varphi^*(r-\rho)H\varphi(r) = -\gamma, \tag{1.27}$$

and as the first-order energy (ϵ_k) is provided by $\langle k \mid k\rangle = 1$, then is obtained that:

$$\langle k \mid H \mid k\rangle = -\alpha - \gamma\sum_{j} exp(-ik\cdot\rho_m) = \epsilon_k. \tag{1.28}$$

The dependence of the overlap energy γ on the interatomic separation ρ can be evaluated explicity for two hydrogen atoms in 1s state. In Rydberg energy units, $Ry = me^4/2\hbar^2$, the overlapping energy is given by:

$$\gamma(Ry) = 2(1 + \rho/a_0)exp(-\rho/a_0), \tag{1.29}$$

where $a_0 = \hbar^2/me^2$. The overlap energy decreases exponentially with the separation.

1.3 KWANT software

Kwant is a free (open source) Python package for numerical calculations on tight-binding models with a strong focus on quantum transport. It is designed to be flexible and easy to use to solve scattering problems in a robust and highly efficient way. The tight-binding method of modelling lies between the very accurate, expensive and fast but limited empirical ab initio methods.

The tight-binding methods describe a vast variety of system and phenomena in quantum physics such as:

1. Metals
2. Graphene
3. Topological Insulator
4. Quantum Hall Effect
5. Conductance
6. Superconductivity
7. Spintronics
8. Molecular electronics
9. Any combination of the above, and many other things

The definition of a physical system amount to writing a simple python program that operates with physical parameters or concepts, such as lattices, shapes, symmetries, and potentials. The form one writes the Hamiltonian for the systems in KWANT is very

close to what one would write on a blackboard. In the tight-binding approximation, the Hamiltonian can arise directly from an atomic description of a physical system, in which the sites could correspond to atoms or molecules. In this sense, KWANT has two important sections which allow us to describe the system and adopt it to different situations, these are:

1. Scattering section in which it is defined what kind of imperfections the system has. At the moment to define the system, for example, it could be a perfect system for which any kind of impurities, vacancy or imperfections affect to the transport, to a more realistic system for which the position of each atom in the structure could affect the conductance. Also scattering section is defined as hopping, that is simply a tuple of two of sites, which defines an edge of the graph that makes up a tight-binding model.

2. Leads section that within the Landauer-Buttiker formalism these leads act as wave guides leading plane waves into and out of the scattering region and correspond to the contacts of a quantum transport experiment.

The implementation of different tight-binding models in KWANT opens a wide range of possibilities to calculate in quantum transport or other branches. To visualize this concept, we consider the simplest tight-binding model implemented in KWANT (for default) that is related to a system with no impurities and in which the interactions are given for the nearest neighbors in the system. The simplest Hamiltonian is given by the two dimensional Schrödinger equation:

$$H = \frac{-\hbar^2}{2m}(\delta_x^2 + \delta_y^2) + V(y), \tag{1.30}$$

with a hard-wall confinement $V(y)$ in the y direction.

To be able to introduce this model into KWANT, the continuous Hamiltonia described in 1.30 is discretized thus turning it into a tight-binding model. For simplicity, the

hamiltonian is discretized on the sites of a square lattice with lattice constant a. Each site with the integer lattice coordinates (i, j) has the real-space coordinates $(x, y) = (ai, aj)$. Introducing the discretized positional states as:

$$\mid i, j\rangle = \mid ai, aj\rangle = \mid x, y\rangle, \tag{1.31}$$

the second-order differential operators can be expressed in the limit when $a \longrightarrow 0$ such as:

$$\delta_x^2 = \frac{1}{x^2}\sum_{i,j}(\mid i+1, j\rangle\langle i, j \mid\mid i, j\rangle\langle i+1, j \mid -2 \mid i, j\rangle\langle i, j \mid), \tag{1.32}$$

as an equivalent for δ_y^2. Substituting them in the Hamiltonian it is obtained:

$$\begin{aligned} H = & \sum_{i,j}[(V(ai, aj) + 4t) \mid i, j\rangle\langle i, j \mid -t(\mid i+1, j\rangle\langle i, j \mid + \mid i, j\rangle\langle i+1, j \mid \\ & + \mid i, j+1\rangle\langle i, j \mid + \mid i, j\rangle\langle i, j+1 \mid)], \end{aligned} \tag{1.33}$$

with $t = \hbar^2/2ma^2$. For finite a, this discretized Hamiltonian approximates the continuous one to any required accuracy. The approximation is good for all quantum states with a wavelength considerably larger than a. The Hamiltonian derived in (1.33) describes almost any system, either in 1D, 2D or 3D. This tight-binding model is the general Hamiltonian implemented by KWANT to calculate transport in the simplest models (linear, square and cubic). However, to implement the different tight-binding models with another kind of interactions in more complicated systems make KWANT a useful computational tool for quantum transport, allowing to simulate many physical and chemical experiments in which the use of computational tools allows to determine if theoretical or experimental approaches are working as the expected.

1.4 Atomic interactions

1.4.1 Atomic Spin-Orbit interaction

The Spin-Orbit (SO) interaction is the coupling between the spin of the electron and its orbital motion around the nucleus. When an electron moves in the finite electric field of

the nucleus, the SO interaction causes a shift in the atomic energy levels of the electron due to the electromagnetic interaction between the spin of the electron and the electric field. In the rest frame of the electron, there exist a magnetic field created by the interaction of the angular momentum of the electron and the electric field of the nucleus [22].

The equation for the energy splitting ($\Delta\xi$) due to spin-orbit interaction was first derived in 1926 by Llewellyn Thomas, using Bohr model of the hydrogen atom, Schrödinger quantum mechanics, and relativistic kinematics. These results turned out to be complete agreement with the predictions of Dirac relativistic quantum mechanics, which was formulated

two years later (1928) [23]. The Thomas result may be written as:

$$\Delta\xi = \frac{g}{4m^2c^2}\frac{dV(r)}{rdr}\mathbf{s}\cdot\mathbf{L}. \tag{1.34}$$

Here, $V(r)$ is the potential energy of the electron at distance r from the nucleus, and $\mathbf{L}$ is the orbital angular momentum of the electron moves in a circular orbit of radius r with velocity $\mathbf{v}$ in the presence of the electric field of the nucleus, according to Bohr classical model.

The Hamiltonian for the coupling of the electron spin with an external magnetic field is $\mathbf{H} = \boldsymbol{\mu_s}\cdot\mathbf{H}$. In the rest frame of an electron in orbit around a nucleus, an additional magnetic field is present due to the electric field E generated by the charge of the proton in its rest frame, in which the electrical potential of the nucleus is $V(r) = Ze/r$, so $E = Zer/r^3$ [6]. This electrical field is Lorentz transformed into a magnetic field in the electron rest frame. The magnetic field $\mathbf{H_{add}}$ in the moving frame of the electron is given by:

$$\mathbf{H_{add}} = -\frac{\mathbf{v}}{c}\times\mathbf{E} = -\frac{\mathbf{p}}{mc}\times\mathbf{E}, \tag{1.35}$$

That is, the magnetic field that results in the electron rest frame from the transformed static electric field is given by equation (1.35). Using this magnetic field in the expression

$\mathbf{H} = -\boldsymbol{\mu_s} \cdot \mathbf{H}$, resulting in the spin-orbit Hamiltonian by substituting the magnetic field in equation (1.35) resulting in:

$$\mathbf{H_{SO}} = -\mu_s \cdot \mathbf{H_{add}}/2. \tag{1.36}$$

The factor of 1/2 is due to the fact that the rest frame of the electron is not an inertial frame, hence, the Hamiltonian needs to be corrected to account for the fact that the electron is an accelerating frame. An electric field with a component perpendicular to the electron velocity causes an additional acceleration of the electron perpendicular to its instantaneous velocity, leading to a curved electron trajectory moves in a rotating frame of reference, and this provides additional electron precession is half the naive result. After substituting (1.35) into (1.36) and using $E(r) = Zer/r^3$, the following equation is:

$$H_{SO} = \mu_{\mathbf{s}} \cdot \frac{\mathbf{p}}{mc} \times (Zer/r^3)/2 = \frac{Ze^2}{2m_e^2c^2r^3}\frac{\hbar}{2}\boldsymbol{\sigma} \cdot \mathbf{L}, \tag{1.37}$$

where $\mu_s = -g_s\mu_B(S/\hbar)$ and $\mathbf{L} = \mathbf{r} \times \mathbf{p}$ were used. This spin-orbit Hamiltonian is often written in the form:

$$\mathbf{H_{SO}} = \xi(r)\frac{\mathbf{L} \cdot \mathbf{S}}{\hbar^2}, \tag{1.38}$$

where $\xi(r) = \frac{Ze^2\hbar^2}{2m_e^2c^2r^3}$ is the spin-orbit coefficient of the electron and it has units of energy [6]. Spin–orbit coupling is important in many semiconductors. Consider an electron with effective mass m^* in a solid, subject to a potential $V(r)$. The potential induces an electric field $\mathbf{E} = \mathbf{rV/e}$ which, in turn, generates SO coupling. The SO Hamiltonian is:

$$H_{SO} = \lambda[\mathbf{r}V \cdot (\mathbf{p} \times \boldsymbol{\sigma}) + (\mathbf{p} \times \boldsymbol{\sigma}) \cdot \mathbf{rV}], \tag{1.39}$$

where $\mathbf{p} = -i\hbar\mathbf{r}$ is the momentum operator, $S = \hbar\sigma/2$ is the spin operator and

$$\lambda = -\frac{\hbar}{8(m^*)^2c^2},$$

is the spin-orbit strength. The magnitude of the SO coupling depends on the speed of the electrons and the strength of the electric field acting on it, as well as on its effective mass, m^*. Large SO interaction is obtained when the Bloch electrons move close to the

nuclei with velocities that are close to relativistic, and for which the effective mass of the electrons is small.

The potential experienced by an electron in a crystal includes the periodic crystal part $V_c(r)$ and an "external" potential $V_{ext}(r)$ due to imperfections and any other external fields, $V(r) = V_c(r) + V_{ext}(r)$. Both parts affect to the SO coupling, since the electric field in H_{SO} is the gradient of the full potential. The single-particle Hamiltonian including SO is

$$H = -\frac{\hbar^2}{2m^*} \bigtriangledown^2 + V(r) + H_{SO}. \tag{1.40}$$

It is useful to incorporate all the terms having the symmetry of the crystal into one term, which includes the intrinsic (crystal field related) SO potential,

$$H_c \equiv -\frac{\hbar^2}{2m^*} \bigtriangledown^2 + V_c(r) + \lambda[\mathbf{r}V \cdot (p \times \sigma) + (p \times \sigma) \cdot \mathbf{r}V]. \tag{1.41}$$

Let us consider electrons in a cubic direct gap semiconductor, where the energy has a minimum at the center of the Brillouin zone, k=0. Because the spin-orbit interaction is even under time reversal, each level is at least two-fold degenerate (Kramers theorem). At k=0, this is the only degeneracy. The two states corresponding to this degenerate level are referred to as a Kramers doublet. We can write an effective Hamiltonian for the system as

$$H_{eff} = E_n(k) + H_{int} + \lambda[\mathbf{\Delta V_{ext}}(\mathbf{r}) \cdot (\mathbf{p} \times \boldsymbol{\sigma}) + (\mathbf{p} \times \boldsymbol{\sigma}) \cdot \mathbf{\Delta V_{ext}}(\mathbf{r})], \tag{1.42}$$

where the spin-orbit energy due to the periodic potential is:

$$H_{int} \equiv \mu_B \mathbf{h}(\mathbf{k}) \cdot \sigma, \tag{1.43}$$

with $\mathbf{h}(\mathbf{k})$ being the SO intrinsic field that depends on the details of the crystal structure, $\mathbf{h}(\mathbf{k})$ has units of energy/magnetic- field, and is $\mathbf{k}$-dependent. Note that the time-reversal operation takes $\sigma \Rightarrow -\sigma$ and $k \Rightarrow -k$. Hence $h(k) \Rightarrow -h(-k)$, so that the intrinsic

Hamiltonian H_{int} is time-reversal invariant. In crystals with inversion symmetry, where $h(k) = h(-k)$, the intrinsic spin-orbit field must vanish.

The intrinsic spin-orbit coupling $h(k)$ defined through equation (1.43) is equivalent to a local magnetic field related to the band structure. $\mathbf{h}(\mathbf{k})$ depends strongly on crystal symmetry and is different for electrons and holes. It also depends on space dimension $d = 2$ or $d = 3$. In a static situation, the particle magnetic moment tends to align along $h(k)$. When an electric field $\mathbf{E} = E\hat{\mathbf{x}}$ is applied, the vector k evolves in time according to the semi classical equations $\mathbf{k} = eE/\hbar$, and consequently, the effective field $h(k)$ evolves according to $h(k) = \Delta_k \mathbf{h}(\mathbf{k}) \cdot e\mathbf{E}/\hbar$. For weak electric fields, the adiabatic approximation is justified. Then, the effective magnetic field $h(k)$ varies slowly with time, and the electron has enough time to adjust its spin to lie along $h(k)$,there by undergoing spin precession [6].

1.4.2 Rashba effect

In 1984, Bychkov and Rashba introduced a simple form of spin–orbit coupling to explain the peculiarities of electron spin resonance in two-dimensional semiconductors [24]. Rashba effect is a momentum-dependent splitting of spin in bulk crystal. In crystal that lack an inversion centre, electronic energy bands are split by SO coupling. More specifically, in non-centro symmetric zinc-blende or wurtzite semiconductors, bulk SO coupling becomes odd in the electron's momentum p, as originally realized by Dresselhaus and Rashba. Dresselhaus was the first to notice that in zinc-blende III–V semiconductor compounds lacking a centre of inversion, such as GaAs or InSb, the SO coupling close to the Γ point adopts the form:

$$\hat{H}_{D_3} = (\gamma/\hbar)\left[(p_y^2 - p_z^2)p_x^2\sigma_x + c.p.\right], \tag{1.44}$$

where c.p. denotes circular permutations of indices. Of course, additional symmetry considerations in the band structure result in additional odd-in-p SO coupling terms. In

the presence of strain along the (001) direction, the cubic Dresselhaus SO coupling given in equation (1.44) reduces to the linear Dresselhaus SO coupling:

$$\hat{H}_R = (\alpha_R/\hbar)(\mathbf{z} \times \mathbf{p}) \cdot \sigma, \tag{1.45}$$

where α_R is known as the Rashba parameter. In other words, in the solid state the Dirac gap $mc^2 \approx 0.5$ MeV is replaced by the energy gap ~ 1 eV between electrons and holes, and $\alpha_R/\hbar >> \mu_B E_z/mc$. This convenient form, derived for 2D plane waves, is only phenomenological and must be applied with precaution to realistic systems. Indeed, theoretical investigations showed that the lack of inversion symmetry does not only create an additional electric field E_z,but also distorts the electron wavefunction close to the nuclei, where the plane-wave approximation is not valid [25].

The recent discovery of the Rashba effect in the two dimensional electron gas (2DEG) systems such as perovskite surfaces and interfaces has led to the possibility of tuning its properties by external electric fields. The study of the Rashba effect in 2DEGs is of interest not just from a fundamental point of view, but also due to potential applications in spintronics devices [24].

1.5 DNA MODEL

DNA was discovered by Watson and Crick in 1953 and since then its discover to our days it has transformed the foundations of biology, chemistry, medicine and many others areas related to them. DNA is a natural-occurring polymer that plays a central role in our life, many unique properties of DNA have inspired a search for its non-biological applications. DNA is an organic polymer of four different monomers where each monomer is composed of a phosphate group, a single-ring sugar and one of four bases: Adenine (A) , Thymine (T), Cytosine (C) and Guanine (G) (Figure 1.7). The bases are planar single or double ring aromatic compounds. The monomers can form bonds between the sugar and the phosphate and form into a long polymer or strand of DNA. The bases can also interact

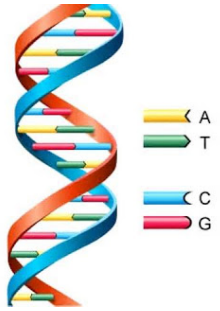

Figure 1.7: Structure of DNA

with each other through the formation of hydrogen bonds, specifically, A-T and G-C pairing. An entire strand of DNA can form base-pairs with a complementary strand to make double-stranded DNA [26].

The chirality of the sugars and the optimization of hydrogen bond angles leads to the formation of a regular helical structure for DNA, with 10.4 base pairs per turn, the length of hydrogen bond are approximately 3 Å which is larger than the typical covalent bond that connects neighboring atoms in a base, which is about 1.3 - 1.5 Å. The turn of each strand, in which contains the bases, which is called "pitch" is chose around 35.4 Å, and the angle between two consecutive base pairs is 34.6°, according to the configuration B-DNA [27].

The control of electron spin transport in molecular systems with chirality, like DNA, has been receiving a lot of attention among different scientific communities mainly because of possible applications in spintronics and for understanding of the spin effects in biological systems.

From the discovering of the spin-conductance and spin-selectivity in chiral organic molecule several approaches have been developed, analytical and numerical either in DNA or thin chiral organic molecules [11, 12, 13, 28]. Research reports presented in[11] and [13] assume that the spin-selectivity is given by the scattering of the free electrons and their transport bound to the helix. This scattering potential contains a confining term and a spin-orbit contribution that are responsible for the spin-dependent scattering of electrons,

deriving the spin-orbit from the intrinsic atomic spin-orbit if the outer p orbitals of the carbon atoms. In the other point of view [28], and [12] explain the spin-selective transport of electrons through of helical shaped electrostatic potential, assuming two main factors to explain for the selectivity of spin: modified Rashba-like spin-orbit interaction, reflecting the helical symmetry of the system, and a weakly dispersive electronic band of the helical system.

These theoretical approaches have shown the spin-selective transport of electrons through two regimes: (i) free electrons scattering off the atomic orbital potentials and (ii) electrons bound to move between atomic orbitals along the double helix in the molecular electrostatic potential. All the proposals have to fix the spin orbit coupling strength in order to fit the experimental results as they did not derive the effective values from a more detailed model of the molecule.

In 2016, Varela and collaborators developed an analytical model of DNA to explain the spin filtering and chiral spin transport in these molecules [9, 29]. In their work, they consider a double-helix DNA type-structure in which each base is represented by a p-like orbital projected perpendicular to it and bonded s and p orbitals on the molecular base plane, representing a carbon atomic outer shell. Bases are paired forming a step on a staircase and that are separated by a distance close to the double-helix diameter. Considering the atomic spin-orbit interaction and the Rashba effect on the electric dipoles of the hydrogen bonding between the bases, they obtained an effective tight-binding Hamiltonian to connect p_z orbitals in neighboring sites labeled by $\imath$ and $\jmath$, given by :

$$H = \sum_{\langle \imath\jmath \rangle}^{intra} c^{\dagger}(t^{in} + i\lambda_{SO}\nu_{\imath\jmath}s_y + i\lambda_R^x\nu_{\imath\jmath}s_y)c_{\jmath} + \sum_{\langle \imath\jmath \rangle}^{inter} c_{\imath}^{\dagger}t^{out}c_{\jmath}, \tag{1.46}$$

where $\nu_{\jmath\imath} = sgn(\jmath - \imath)$, the sum *intra* is on the neighboring bases in the same helix and the sum *inter* is on bases in different helices. The first term in each sum correspond to the kinetic energy, and the following terms represent the greatest contribution in the intrinsic spin-orbit and Rashba interactions due to the coupling between atomic SO and the electric

field of hydrogen bonds, respectively. They estimated values for the interactions, such that $t^{in} = t^{out} = -10meV$; $\lambda_{SO} = 0.671$ meV and $\lambda_R^x = 3.6$ to 20 meV.

In order to determine if the Hamiltonian developed in (1.46) explain successfully the spin-selective transport of electrons in DNA, computational programs based on tight-binding models are carried out, so in this way, compare with the experimental and conclude if the theoretical approach of an intrinsic spin-orbit and its interactions are the responsible for this filtering in this kind of molecules.

CHAPTER 2

RESULTS

In order to study quantum transport in different systems, we must use KWANT which is described in Section 1.2.1. This software will allow us to obtain conductance and band structure which are the main parameters required to study the quantum transport in different systems through tight-binding models.

2.1 Linear chains

2.1.1 1D case

For this case we want to simulate a linear chain of 30 atoms that represent the scattering region using metallic leads. Linear chain is simulated with no presence of imperfection or impurities within the system and leads behave as metallic, a ballistic system. The tight-binding Hamiltonian is written as:

$$H = \frac{-\hbar^2}{2m}\delta_x^2 + V, \tag{2.1}$$

where V is the external potential. Assuming a linear chain growing in x direction, then:

$$\mid i\rangle = \mid ai\rangle = \mid x\rangle, \tag{2.2}$$

being a the lattice parameter. The second-order differential operators can be expressed in the limit $a \longrightarrow 0$ as:

$$\delta_x^2 = \frac{1}{x^2}\sum_i (\mid i+1\rangle\langle i \mid + \mid i+1 \mid -2 \mid i\rangle\langle i \mid). \tag{2.3}$$

Substituting (2.3) in (2.1) we obtain the Hamiltonian:

$$H = \sum_i [(V(ai)+4t) \mid i\rangle\langle i \mid -t(\mid i+1\rangle\langle i \mid + \mid i\rangle\langle i+1 \mid + \mid i\rangle\langle i \mid + \mid i\rangle\langle i \mid)] \tag{2.4}$$

with

$$t = \frac{\hbar^2}{2ma^2}.$$

The Hamiltonian obtained in (2.4) is a tight-binding Hamiltonian which represent the interaction of an atom with its neighbors. This is the input Hamiltonian introduced in KWANT code that can be seen in Appendix A.1.

The evaluated system, shown in the Figure 2.1, correspond to a linear chain of 30 atoms, represented by blue atoms, that are the scattering region, and red points, that are the leads from which the electrons are being injected. The output obtained with Hamiltonian used in equation 2.4 is sown in Figure 2.1 (B.) in which is observed that the Fermi Energy versus the conductance exhibit a constant behavior. The behavior observed seems to correspond to a ballistic (no resistant), which is explained for the size of the linear

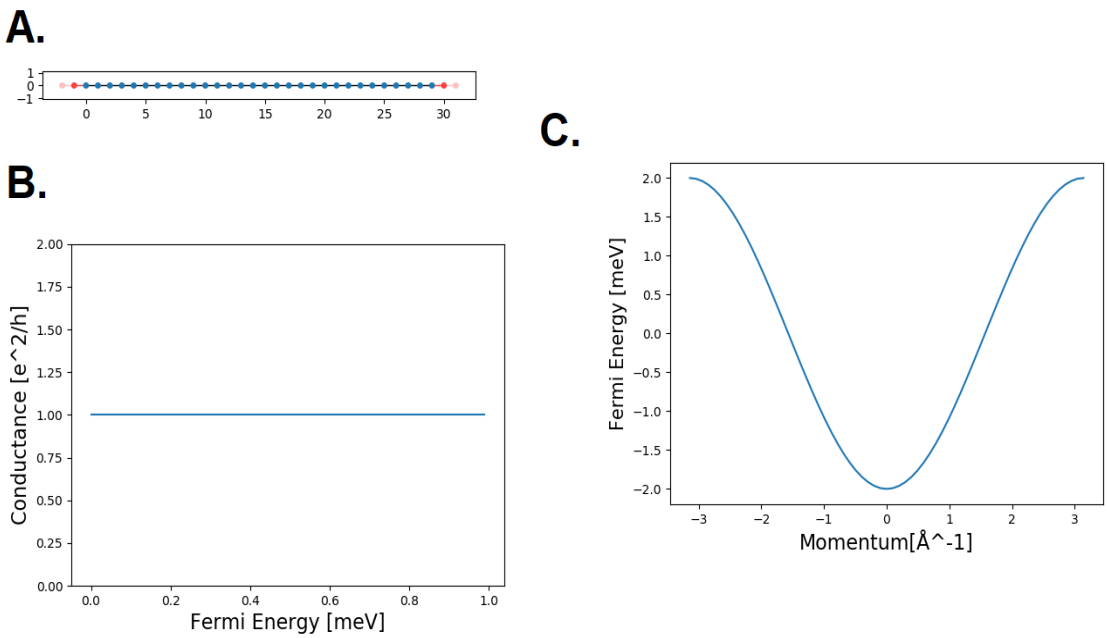

Figure 2.1: **A.** Representation of a linear chain of 30 atoms. **B.** Conductance for a linear chain of 30 atoms (no impurities) as a function of the Fermi Energy. **C.** Band structure of a linear chain of 30 atoms

chain. Finally, the band structure is shown in Figure 2.1 (C.), exhibits levels of energy accepted for the system, that is, zero impurities. All energy range is accepted with no band gap presented, proving that the conductance is confirmed using the band structure.

2.1.2 2D case

In this case, a 2D system, such as a quantum wire, is simulated assuming that electrons injection into the system is by metallic leads. For this system, the transmission probability and band structure are obtained in order to describe its characteristics.

The tight-binding Hamiltonian describing the system is given by:

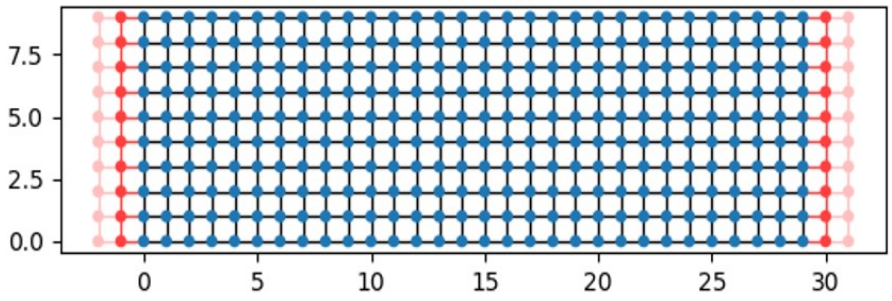

Figure 2.2: **a.** 2D system of 30 atoms length and 10 atoms of height. The blue points correspond to the scattering region and red points are the leads.

$$\begin{aligned} H &= \sum_{i,j}[(V(ai,aj)+4t) \mid i,j\rangle\langle i,j \mid -t(\mid i+1,j\rangle\langle i,j \mid + \mid i,j\rangle\langle i+1,j \mid \\ &\quad + \mid i,j+1\rangle\langle i,j \mid + \mid i,j\rangle\langle i,j+1 \mid)] \end{aligned} \tag{2.5}$$

with $t = \hbar^2/2ma^2$. The Hamiltonian derived in (2.5) is the input tight-binding model for 2D model to be introduced in KWANT (Appendix A.2).

A 2D system is performed in x and y directions considering a chain with 30 atoms of length and 10 atoms of height (Figure 2.2). The conductance curve, and the band structure are shown in Figure 2.3. The conductance quantized units are e^2/h and its value is determined by the number of occupied sub bands that increase with energy, each stair observed is related to a sub band different yield to the conductance in the system. Band structure represented in Figure 2.3 shows all the band related to each sub-band present in the system. For each band there is a stair in conductance, it is argued to that each band represent another available state to transport electrons within system. The parabolic behavior showed in the band structure is as a consequence of that all the bands are simulated as a metallic lead, which exhibit a band structure with no band gap or disturbance present.

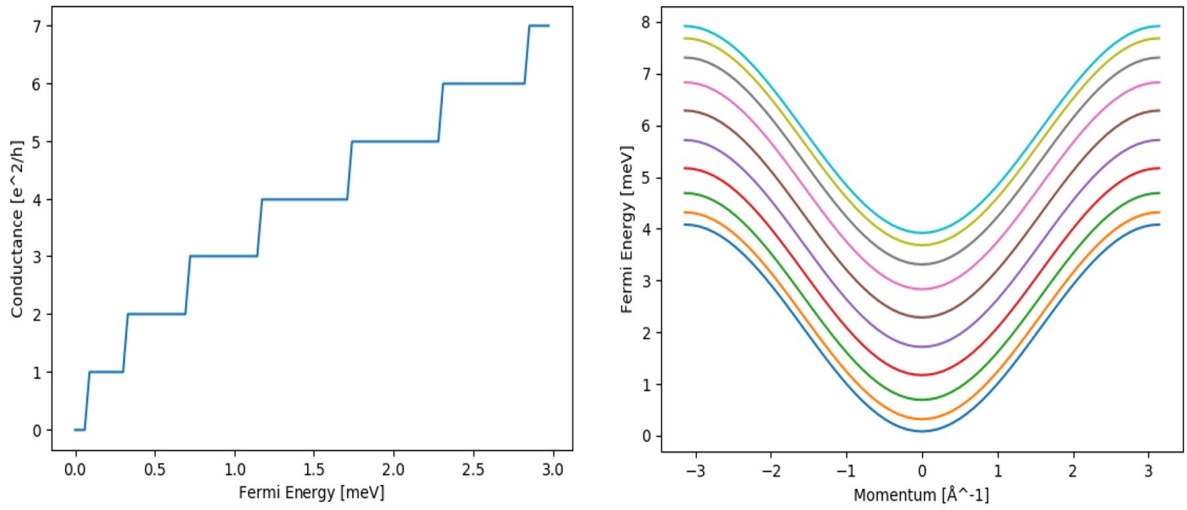

Figure 2.3: The conductance and band structure for a 2D system.

2.1.3 Regimen of Transport

The example shown in the Section 2.1, that represented for a linear chain of 30 atoms, is not enough to show the efficiency of KWANT to calculate transport phenomena. As is suggested in equation (1.22) of Section 1.2, the relation between the conductivity and the length, correspond to a decay exponential. In the previous Section 2.1.1, a representation of a linear chain was made, however, to observe the dependence of the conductivity as a function of the length it is necessary to perform an average of many linear chains. The ensemble of particles can be made by the average of many microscopic configurations. So, in this way, calculating the conductivity of a section positions will be the sum of all the previous conductivities performed before. To show this concept, we have calculated the conductivity of a linear chain from 30 atoms to 6000 atoms.

In Figure 2.4 (A) and (B) are shown plots of the conductivity versus the length of the chain for numerical results obtained and that suggested by theory. As expected in the calculus of an average of linear chain with the increasing of the length of the chain the conductivity is going to decrease exponentially showing different regimen of transport, from ballistic to diffusive and ending in Anderson localization, which is expected, and its

behave seems to correspond to the exposed in the equation 1.22. Notice that the graph performed for KWANT very similar to the suggested in the literature and shows that the quantum transport in mesoscopic systems can be calculated computationally [18].

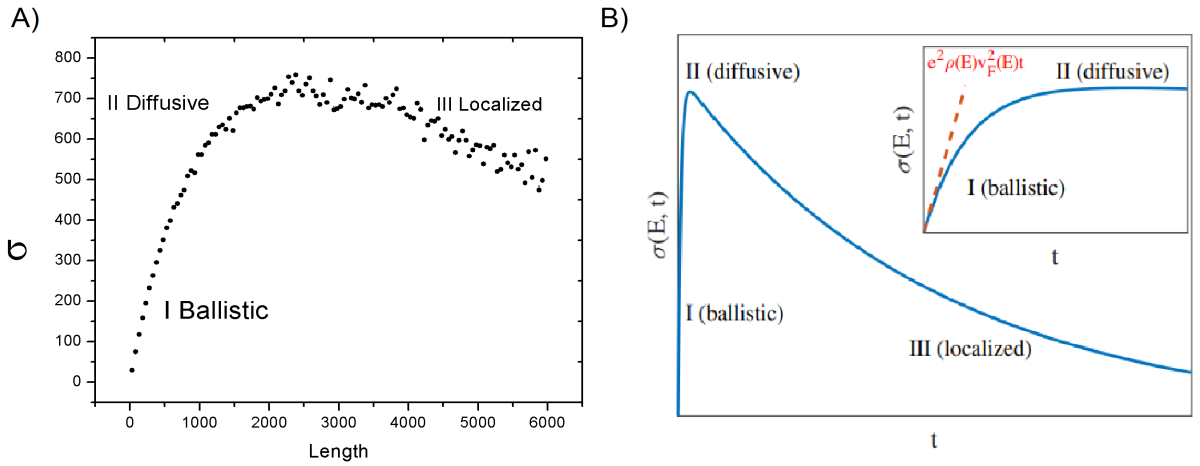

Figure 2.4: **A.** Graph of the conductivity versus length obtained in this work. **B.** Theoretical graph of the conductivity versus length [18].

The huge increase in computational power available for scientific purpose in the last decades has led to a proliferation of computational methods. In the field of atomistic modelling, computational facilities led to the development of schemes which retained the essential quantum mechanical basis, but greatly reduced the computational time required [17].

2.2 3D DNA MODEL

In this seccion, the behavior of the conductance and band structure for more complex structure, DNA molecule is analyzed. To model the DNA, a doble helix structure is considered, in which all the nitrogenous bases are represented as hard spheres, which have same orbitals (π orbital), separated by a angle that depends on the number of base pair.

The position vector for each base in a single helix is labeled with R_i, where i is the label for the number of sites such that $i = 1.....N$, being N the total number of bases in a single helix. The bases in the other helix are labeled by $R_i^{'}$. Thus, the pair of labels R_i and $R_i^{'}$ represent a pair at the site i. If b is the pitch of the molecule and $\Delta\theta$ the angle between two consecutives bases of the same helix, the vectors R_i and $R_i^{'}$ can be written in the form:

$$R_i = acos[\varphi + (i-1)\Delta\theta]\hat{X} + asin[\varphi + (i-1)\Delta\theta]\hat{Y} + \frac{(i-1)\Delta\theta}{2\pi}b\hat{Z}. \tag{2.6}$$

The other helix $R_i^{'}$ is constructed with $\varphi = 180°$. It indicates that both helix are dephased by 180^o from each other.

If N base pairs are considered, such that each turn $\mathcal{N}$ of the helix contains M base pairs spaced by the angle $\Delta\theta$, the following relations are fulfilled:

$$\mathcal{N} = \frac{N-1}{M-1} \tag{2.7}$$

$$\Delta\theta = \frac{2\pi}{(M-1)}. \tag{2.8}$$

Using the parameters mentioned before, the first simulation of DNA using KWANT was performed, taking into account the following parameters:

- b (pitch) = 35.4 Å
- M (number of pairs) = 10
- $\varphi = 180°$
- $\Delta\theta = 40^o$,

All the parameters used are mentioned in the Section 1.5, and the angle is calculated with equation 2.8, in addition, it was made considering the SO intrinsic coupling, a Rashba effect and magnetic and no-magnetic leads.

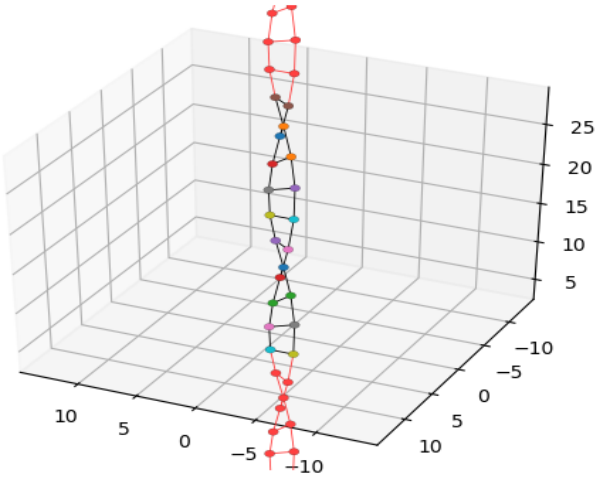

Figure 2.5: 3D DNA, leads DNA

The tight-binding model used for this simulation is the one indicated in the equation (1.46) which is:

$$H = \sum_{\langle \imath\jmath \rangle}^{intra} c^{\dagger}(t^{in} + i\lambda_{SO}\nu_{\imath\jmath}s_y + i\lambda_R^x\nu_{\imath\jmath}s_y)c_\jmath + \sum_{\langle \imath\jmath \rangle}^{inter} c_i^{\dagger}t^{out}c_\jmath.$$

The 3D system simulating DNA is shown in the Figure 2.5. In this model each pair is simulated by points of different color, and the red points are the leads. An idea of how this positions and parameters are introduced into the program are given in the Appendix A.3, showing some lines of code used to start to define some parameters mentioned before.

By using KWANT it is required to define the leads connected to the system under study, which are the main donator of electrons in the structure depending in the number of modes that the leads have. In other words, the greater the number of modes the greater the availability of states that can be accepted by the structure. The leads considered in this study have the same DNA form because the band structure or the state in which

are available for transporting were needed to know. Furthermore, the DNA and leads are oriented in z direction, that matches the direction of transport in [9].

2.2.1 No ferromagnetic leads, with and without SO interaction

In Figure 2.6, the band structure (left) and the conductance or transmittance (right) of the DNA system are shown for the case in which no spin-orbit interaction and no ferromagnetic lead has been taken into account. In the plots bands degenerated in spin can be seen, it means, for each band (or line) there are two bands overlapping, one for each electron. For the conductance plot, two regions are observed, one from -10 to 10 meV and the second region represents the rest of the graph. The conductance associated with the first region is double that for the second one, it can be explained according to the band structure obtained. At a Fermi energy of -20 meV two bands are passing, one with positive Fermi velocity (goes up) and other with negative Fermi velocity (goes down), then the band which goes up gives the electrons are propagating to the right meanwhile the band which goes down the electrons propagating to the left. However, in the first range (-10 to 10 meV) there are two bands with positive Fermi velocity (goes up), due to the degeneracy of spin that provides the double of electrons contributing to the transport. This is clearly shown in the graph of conductance. For the of no spin-interaction and no ferromagnetic leads exists a degeneracy of the spin in the system and the study of this band give an important characteristic of the system.

To visualize the spin-orbit interaction in the system, calculations different values for terms associated with spin-orbit intrinsic and Rashba effect were carried out, with the intention of understand how the intensity of these interactions acts inside the system. Using this premise, 4 band structures have been evaluated to study how the intensities of these interactions affect to the band structure, relating them later to the selectivity of spin in DNA. In Figure 2.7 4 different band structure graphs for different spin-orbit intensities are shown, for which there is no presence of a ferromagnetic lead. For a better

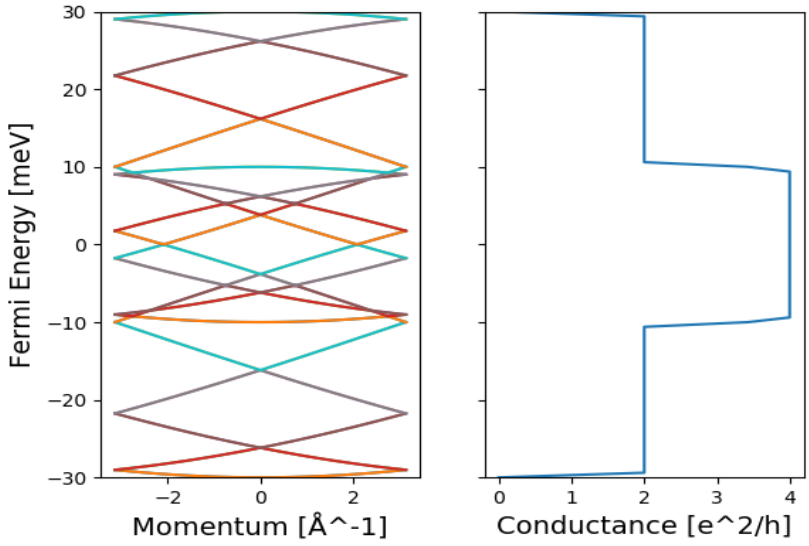

Figure 2.6: Band structure and conductance in DNA system. No spin-orbit interaction and no-ferromagnetic leads are considered.

visualization of this case, the range of the graphs was enclosed between -10 to 10 meV due to in this region there are more available states to study and explain the degeneration of spin observed in the plot shown in the Figure 2.6.

The band structures were tested for different intensities of the SO interactions considered in the Hamiltonian and results are shown in the Figure 2.7. The graph A is related to a system in which the spin is degenerated, it to say no spin-orbit and no ferromagnetic lead. Due to that the bands are degenerated could not be expected any kind of spin selectivity in this case because the spin up and down are travelling together. When the SO interaction and the Rashba interaction were turn on, just one of them , it was observed the splitting of the band structure, which is associated with the spin degeneration lack (Fig.2.6, graph B and C, respectively). Although the SO intrinsic and Rashba interactions are different in nature, the contribution to the effective Hamiltonian is similar, this explains why the band structures shown in B and C look similar. However, if we turn on both interactions (SO intrinsic and Rashba), for characteristic values of the contributions, it can be seen that the band structure presents a very different form compared with

the case in which the interactions are considered separately (graph D in the Figure 2.7). This behavior indicates that considering the interactions separately may not be enough to obtain all the necessary information to describe the system.

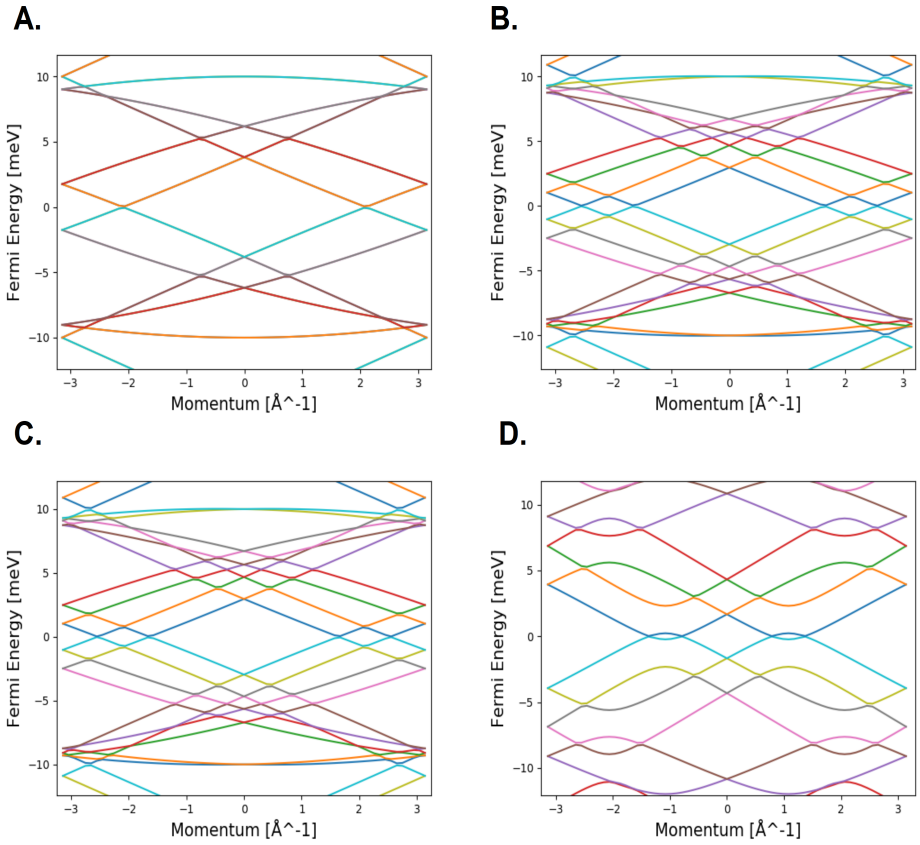

Figure 2.7: Band structures for different spin orbit intensities. **A.** Band structures, no SOC. **B.** Band structures, intrinsic SOC = 0.5 meV, Rashba = 0 meV. **C.** Band structures, intrinsic SOC = 0 meV, Rashba = 0.5 meV. **D.** Band structures, intrinsic SOC = 0.671 meV, Rashba = 10.0meV

Also, calculations of the spin selectivity were carried out for each intensities of SO interactions proposed previously as a function of the Fermi energy. The spin selectivity is a measure of the fraction of electrons with one spin component versus the other component. It is ranged from 0 to 1, where 1 means that the electrons is fully polarized (all spin components are in the same direction) and 0 means that there is the same proportion of

electrons with spin up versus spin down. The results are presented in the graphs shown in the Figure 2.8.

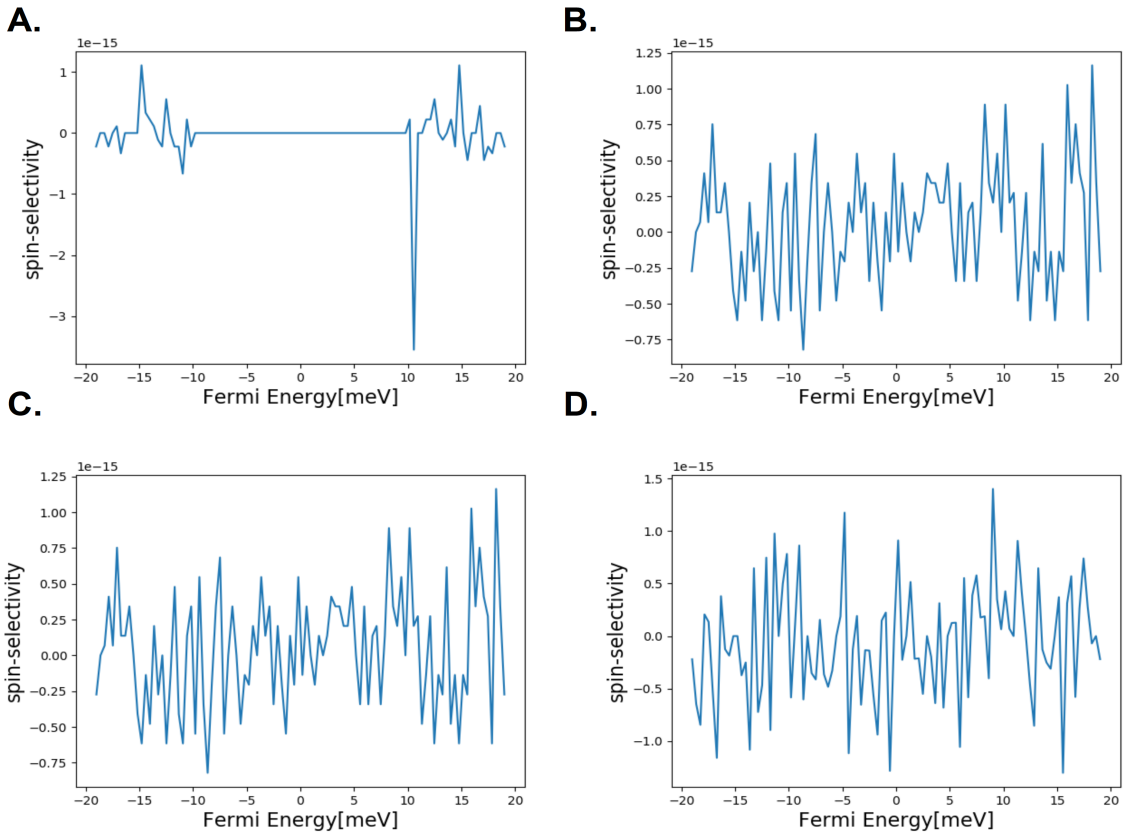

Figure 2.8: Spin selectivity vs Energy for different spin orbit intensities. **A.** Spin selectivity, no SOC. **B.** Spin selectivity, intrinsic SOC = 0.5 meV, Rashba = 0 meV. **C.** Spin selectivity, intrinsic SOC = 0 meV, Rashba = 0.5 meV. **D.** Spin selectivity, intrinsic SOC = 0.671 meV, Rashba = 10.0 meV

For all the graphs it was observed that, regardless of the magnitude of the interaction SO no spin selectivity is observed. The magnitude of the selectivity is in the 10^{-15} order.

2.2.2 Ferromagnetic leads, with and without SO interaction

In the previous cases the electrons are injected as spin up and spin down equally, and once passed through structure, spin up and spin down were detected, assuming a DNA system as

an isolated system. However, KWANT allows to modify the injection of electrons through the use of ferromagnetic leads, injecting spin polarized electrons in both directions (up and down), depending of the intensity of them. In this sense, it was used this to give a direction either parallel or anti-parallel to the spin in the leads and to study the implication of the leads in combination with the SO coupling for visualize the selectivity of spin.

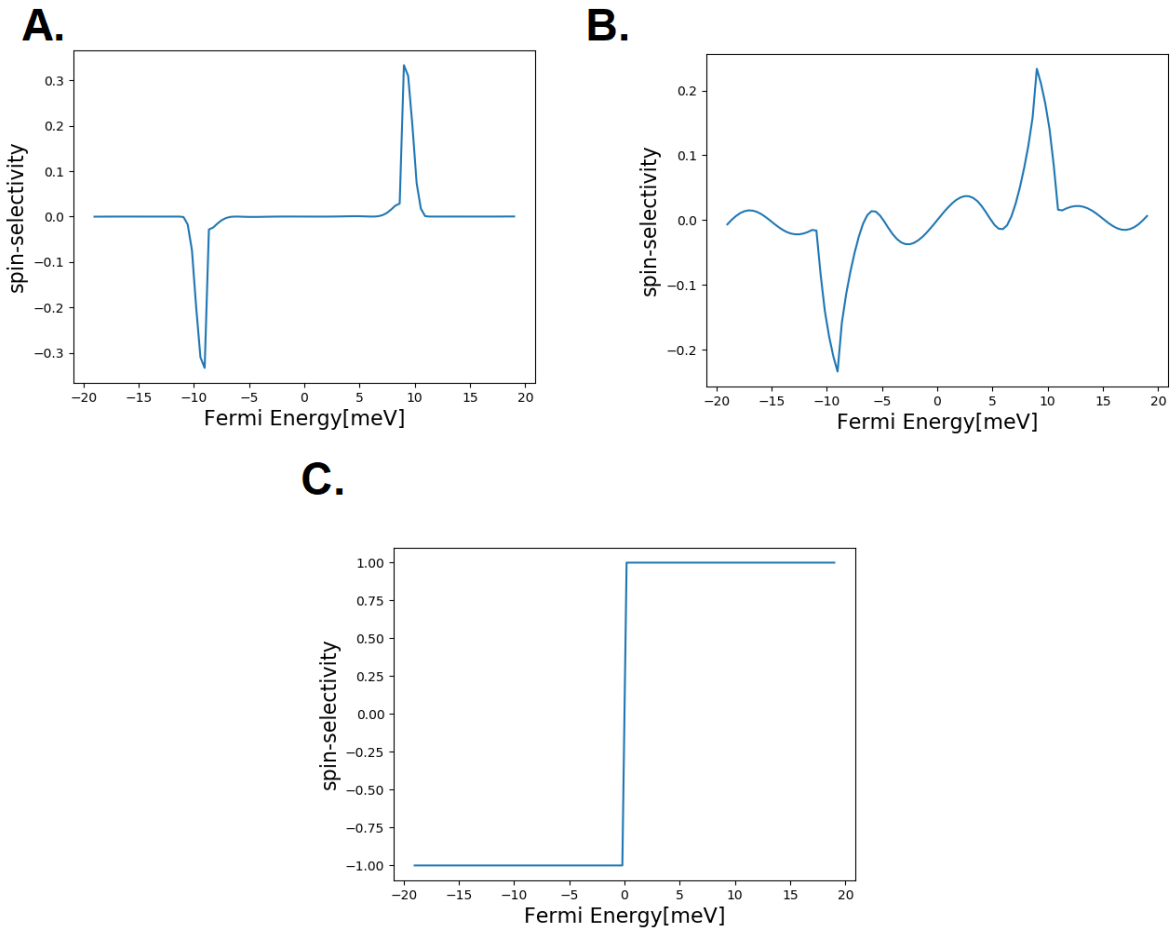

Figure 2.9: Ferromagnetic lead, spin-selectivity vs energy . **A.** Lead onsite = 1 ,no spin-orbit couling. **B.** Lead onsite= 1, intrinsic soc = 1 meV, Rashba= 10 meV. **C.** Lead onsite = 30, intrinsic soc=1 meV, Rashab 10 meV.

In the Figure 2.9 the behavior for the spin selectivity versus Fermi Energy is represented. The graph A is essentially the selectivity of the spin due to the ferromagnetic leads, because SO coupling in the DNA molecule is not present. If the SO interaction

in the molecule is turned on (both intrinsic and Rashba interactions), spin selectivity is observed. This coparision can be seen in the A and B graphs. On the 2.9 (B.) the presence of a wave oscillating around 0 at y axis can be observed, so the direction of the polarization of the spin depends on the Fermi energy.

Finally, for graph C of the Figure 2.9, high value of intensity applied on the lead was used, which obviously generates a polarizability in one direction and presenting very pronounced peak. This means that at large onsite values, the selectivity of the structure depends entirely on the magnetization of the leads, and not on the SO interaction of the molecular structure.

The result shown in the Figure 2.9 is important because it indicates that the SO interaction of the molecule is reflected in spin selectivity only when connected to the ferromagnetic type leads. In the most emblematic experiments, spin selectivity is measured in systems in which at least one of the leads in the outer is magnetic.

CONCLUSIONS

A simulation using KWANT code was carried out, considering a double helix molecule of DNA with all the nitrogenous bases represented as hard-spheres and using a tight-binding Hamiltonian derivated by Varela et al, [9, 29], including intrinsic SO interaction and Rashba effect. From the tested simulations the conductance thought the molecule, the band structure and the spin selectivity were obtained.

1D and 2D linear chains were simulated to corroborate the proper operation of the KWANT code and to analyze its applications in theoretical model. The results obtained for tested systems can be directly compared with those reported in the literature on the general behavior of band structure and conductance. For these linear chains, the different regimens of transport were analyzed, finding that the conductance exponentially decreases when the length of the chain increases to very large values, and it grows very fast with the length, when the length of the chain is small. This result is consistent with the expected behavior according to the theory.

Once proved that the code worked successfully, the scattering region was replaced by a DNA molecule, using tight-binding Hamiltonian proposed by Varela et al, and using KWANT code the conductance of the system, the band structure, and the spin selectivity

were obtained. As expected, if the SO interaction of the molecule is not considered, no splitting is reflected in the levels of the band structure, since these levels are degenerated to the two spin components. The presence of SO interaction and the use of no-ferromagnetic lead indicate that both interactions (intrinsic SO and Rashba effectt) must necessarily be simultaneously considered since the presence of both affect significantly the band structure, which is very different from the structures obtained for the interactions separately. Of course, it should be considered that the magnitude of the interactions also plays an important role and modifies the structure. However, the SO interactions are not enough to evidence spin selectivity in the molecule.

In the other case, when ferromagnetic leadswere used to inject spin-polarized electrons into the molecule, a coupling between the magnetization of the leads and the SO interactions of the molecule was observed in the spectrum obtained for spin selectivity. In fact, the spin selectivity associated with the scattering region was not observed when the SO interaction of the molecule is turned off, even when the leads were ferromagnetic. This result indicates that the nature of the leads can influence the spin selectivity measured in the experiments.

The results obtained in this work are in accordance with those obtained from experimental measures of the spin current for different magnetizations of one of the leads [14], and in which the magnitude of the current translated to spin selectivity can be influenced by leads. The computational code developed for this work can then be adjusted, by conducting experiments where the nature of the leads and their influence on transport is checked.

Finally, the use of the computational tools and package library as KWANT, allows to calculate transport in complex molecules like DNA, obtaining interesting results which can be used in the field of technological applications for the design of spintronic devices with molecular structures.

APPENDIX A

APPENDIX

A.1 Appendix 1

Code implemented to simulate and obtain the conductance for a linear chain of 30 atoms. This code was used for the discussion in section 2.1.1.

```
import kwant
from matplotlib import pyplot

syst = kwant.Builder()
lat= kwant.lattice.chain()
L=30
a=1
t=1.0
#create scattering region
for i in range(L):
    syst[lat(i)]= 0.0
    if i>0:
        syst[lat(i), lat(i-1)]= 1.0
```

```
14
15 sym_left_lead = kwant.TranslationalSymmetry([a])
16 left_lead = kwant.Builder(sym_left_lead)
17 #onsite
18 left_lead[lat(0)]= 0
19 left_lead[lat(1),lat(0)]=-t
20 syst.attach_lead(left_lead)
21
22 sym_right_lead = kwant.TranslationalSymmetry([-a])
23 right_lead = kwant.Builder(sym_right_lead)
24 #onsite
25 right_lead[lat(0)]= 0
26 right_lead[lat(1),lat(0)]=-t
27 syst.attach_lead(right_lead)
28 #Plot
29 kwant.plot(syst)
30 syst=syst.finalized()
31
32 energies = []
33 data = []
34
35 for ie in range(100):
36     energy = ie * 0.01
37     # compute the scattering matrix at a given energy
38     smatrix = kwant.smatrix(syst, energy)
39     # compute the transmission probability from lead 0 to
40     # lead 1
41     energies.append(energy)
42     data.append(smatrix.transmission(1, 0))
```

```
43
44 pyplot.figure()
45 pyplot.plot(energies, data)
46 pyplot.xlabel("energy [t]")
47 pyplot.ylabel("conductance [e^2/h]")
48 pyplot.ylim(0,2)
49 pyplot.show()
```

A.2 Appendix 2

Code used to simulate and obtain the conductance for a 2D system of 30 atoms (length) and 10 atoms (height). This code was used for the discussion in section 2.1.2.

```
import kwant
from matplotlib import pyplot

def make_system (a=1,t=1.0, W=10, L=30):
    lat=kwant.lattice.square(a)
    syst=kwant.Builder()
    #Start with scattering region
    syst[(lat(x, y) for x in range(L) for y in range(W))] = 4 * t

    syst[lat.neighbors()]= -t
    #start to construct the lead
    #construct the left lead
    lead = kwant.Builder(kwant.TranslationalSymmetry((-a, 0)))
    lead[(lat(0, j) for j in range(W))] = 4 * t
    lead[lat.neighbors()] = -t
    #Construct the lead and use the reversed method
    syst.attach_lead(lead)
    syst.attach_lead(lead.reversed())

    return syst

def plot_conductance(syst,energies):
        #Compute conductance
    data=[]
```

```
25      for energy in energies:
26          smatrix = kwant.smatrix(syst, energy)
27          data.append(smatrix.transmission(1, 0))
28      pyplot.figure()
29      pyplot.plot(energies, data)
30      pyplot.xlabel("energy [t]")
31      pyplot.ylabel("conductance [e^2/h]")
32      pyplot.show()
33
34  def main():
35      syst = make_system()
36
37          # Check that the system looks as intended.
38      kwant.plot(syst)
39
40          # Finalize the system.
41      syst = syst.finalized()
42
43          # We should see conductance steps.
44      plot_conductance(syst, energies=[0.03 * i for i in range(100)])
45
46  if __name__ == '__main__':
47      main()
```

A.3 Appendix 3

Code used for DNA simulation. This code show the use of "kwant.lattice.general" which is a parameter used in KWANT to introduce any system no predetermined by the software. In this code we show the position of base pairs and some parameters used to simulate this molecule

```
import kwant
import tinyarray
from numpy import cos, sin, sqrt, pi, tanh

#h_id: helix id
# phi: angular phase between the helices
def PairPosition(n, rho,phi0, xmax):
    r=np.linspace(0,1,n,endpoint=False);
    phi = 2.0*pi*r + phi0
    return np.transpose([rho*cos(phi), rho*sin(phi),xmax*r])

#Define ADN GEOMETRY
LAT = 1.0
RHO = 1.0*LAT;
XMAX= 35.4*LAT;
NUMPAIR=10;
sites_pos = np.array([ PairPosition(NUMPAIR,RHO, phi0, XMAX) for phi0 in
    ↪ (0,pi) ]).reshape(2*NUMPAIR,3)
dna = kwant.lattice.general([(RHO,0,0),(0,RHO,0),(0,0,XMAX)],sites_pos,
    ↪ norbs=2)
dna_sites = dna.sublattices;
Asites= dna_sites[:NUMPAIR];
```

```
21 Bsites= dna_sites[NUMPAIR:];
```

BIBLIOGRAPHY

[1] L. Torsi; M. Magliulo; Kyriaki Manoli and Palaazo. Organic field-effect transistor sensors: a tutorial review. *The Royal Society of Chemistry*, **146**, 2013.

[2] V.K. Mehta and R. Mehta. Objective electrical technology. *Chand (S.) Co Ltd*, **2nd Rev**, 2008.

[3] J. Murray. Out to murray hill to play: An early history of transistors. *IEEE TRANSACTIONS ON ELECTRON DEVICES*, **48**, 2001.

[4] L. Bisiricó and et al. Thin solid films. *The Royal Society of Chemistry*, **520**, 2011.

[5] S. Chikazumi. Physics of ferromagnetism. *Oxford University*, **94**, 1997.

[6] Y. Band and Y. Avishai. Quantum mechanics with applications to nanotechnology and information science. *Elsevier*, **1st ed.**, 2013.

[7] G. Wagnière. On chirality and the universal asymmetry: Reflections on image and mirror. *Wiley-VCH*, **1st Edition**, 2007.

[8] L. Barron. Chiral, magnetism and light. *Nature*, **405**, 2000.

[9] S. Varela; V. Mujica and E. Medina. Effective spin-orbit couplings in an analytical tight-binding model of dna: Spin filtering and chiral spin transport. *Physical Review*, **B00**, 2016.

[10] G. Rikken and E. Raupauch. Enantioselectivity magnetochiral photochemistry. *Nature*, **405**, 2000.

[11] S. Yeganeh; M. A. Ratner; E. Medina and V. Mujica. Chiral electron transport: Scattering through helical potentials. *The Journal of Chemical Physics*, **131**, 2019.

[12] R. Naaman ; R. Gutierrez ; E. D´ıaz and G. Cuniberti. Spin-selective transport through helical molecular systems. *American Physics Society*, **85**, 2012.

[13] E. Medina; F. Lopez; M. A. Ratner and V. Mujica. Chiral molecular films as electron polarizers and polarization modulators. *Europhys*, **99**, 2012.

[14] Z. Xoutie; T. Markus; S. Cohen; R. Gutierrez and R. Naaman. Spin specific electron conduction through dna oligomers. *ACS Chemistry*, **11**, 2011.

[15] C. Kittel. Introduction to solid state physics. *John Wiley Sons Inc.*, **9th Edition**, 1995.

[16] S. Simon. The oxford solid state basics. *Oxford University*, **1st Edition**, 2013.

[17] A. Bestwick. Quantum edge transport in topological insulators. *Stanford University*, , 2015.

[18] D. Supriyo. Electronic transport in mesoscopic systems. *Cambridge University*, , 1995.

[19] D. Feng and J. Guojun. Introduction to condensed matter physics. *Wspc*, , 2005.

[20] R. Romer and M. Schreiber. Numerical investigations of scaling at the anderson transition. in anderson localization and its ramifications. *Springer*, , 2003.

[21] R. Mervyn. The tight binding method. *University of Leicister*, , 2015.

[22] D. Andrews; G.Scholes and G. Wiederrecht. Comprehensive nanoscience and technology. *Academic Press*, **1st ed.**, 2011.

[23] G. Spavieri and M. Mansuripur. Origin of the spin-orbit interaction. *Physica Scripta*, **90**, 2015.

[24] K. Shanavas; Z. Popovic and S. Satpathy. Theoretical model for rashba spin-orbit interaction in d electrons. *Physical Review*, **90**, 2014.

[25] A. Manchon; H. C. Koo ; J. Nitta ; S. M. Frolov and R. A. Duine. New perspectives for rashba spin–orbit coupling. *Nature Materials*, **14(9)**, 2015.

[26] A. Mashaghi and A. Katan. A physicist's view of dna. *Cornell University*, **3**, 2013.

[27] S. Varela and E. Medina. Transporte y polarizaciÓn electrÓnica a travÉs de pelÍculas quirales. *Universidad Central de Venezuela*, , 2016.

[28] Ai-Min Guo and Qin-Feng Sung. Spin-dependent electron transport in protein-like single-helical molecules. *Proceedings of the National Academy of Sciences*, **111**, 2014.

[29] S. Varela;B. Montañes; F López; B. Berche; B. Guillot;V. Mujica and E. Medina. Intrinsic rashba coupling due to hydrogen bonding in dna. *The Journal of Chemical Physics*, **151**, 2019.